Deviations from chain ideality : are they detectable in simulations and neutron scattering of polyisobutylene ?

Julia Zabel

UNIVERSITÉ DE STRASBOURG

Thèse présentée pour obtenir le titre de
Docteur de l'Université de Strasbourg

Discipline : Physique

Deviations from chain ideality: Are they detectable in simulations and neutron scattering of polyisobutylene?

Julia Elisabeth Zabel

Thèse soutenue publiquement le 17 mai 2013

Membres du Jury :

Directeur de thèse :	**J. Wittmer** Directeur de recherche, Institut Charles Sadron, Strasbourg
Rapporteur externe :	**J.-P. Ryckaert** Professeur, Université libre de Bruxelles
Rapporteur externe :	**C. Alba-Simionesco** Directrice de recherche, Laboratoire Léon Brillouin, Saclay
Examinateur interne :	**M. Rawiso** Directeur de recherche, Institut Charles Sadron, Strasbourg
Invité :	**J. Baschnagel** Professeur, Université de Strasbourg

To my daughter,

Henriette Jacobia

Contents

1 | Résumé de la thèse

Introduction

Selon l'hypothèse d'idéalité de Flory, les chaînes de polymères flexibles à l'état fondu se présentent sous la forme de marches aléatoires à trois dimensions, aussi appelées pelotes gaussiennes. Cette hypothèse suppose que toute information relative à la conformation locale (c.-à-d., les angles de liaison ou angles de torsion) subit une décroissance exponentielle le long de la chaîne principale et, par conséquent, n'a aucune influence sur la conformation à grande échelle. De plus, il est avancé que l'écrantage du volume exclu par les chaînes voisines compense tout effet de gonflement. Des expériences de diffusion neutronique (DN) effectuées il y a une trentaine d'années confirment que les polymères adoptent bien des configurations gaussiennes. S'ensuit l'un des piliers de la théorie des polymères : En solution "suffisamment dense" tout polymère flexible peut être décrit comme une marche aléatoire à trois dimensions, indépendamment de sa structure chimique, et ce, après un rééchelonnage adéquat.
Les progrès réalisés dans les domaines des techniques de simulation et de la puissance informatique ont rendu possible l'étude de chaînes très longues. Ceci a permis d'observer de plus près la structure des chaînes de polymère à l'état fondu et révélé une déviation par rapport à la chaîne idéale. Cette déviation est faible, par conséquent un soin extrême est nécessaire pour la distinguer du bruit.

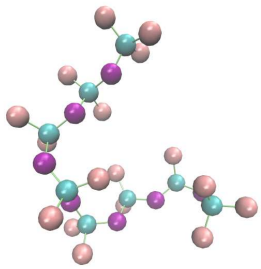

Figure 1.1: Une chaîne PIB simple représentée sous forme d'atomes unifiés. Les groupes de méthyle sont illustrés sous forme de billes orange, les groupes de méthylène sont violets et les atomes quaternaires C sont turquoise. La taille des billes n'a pas été mise à l'échelle.

Jusqu'à présent, la déviation par rapport à la structure gaussienne a uniquement été étudiée dans le cas de modèles à gros grains, par simulation et calcul analytique. La présente thèse cherche à vérifier si ces déviations peuvent également être mesurées à l'aide de simulations atomistiques réalistes et d'expériences de DN modernes.

Modèle de simulation

Nous avons choisi d'étudier le polyisobutylène (PIB) pour plusieurs raisons ; il a été largement étudié et caractérisé par le biais de théories et d'expériences et il fait figure de candidat idéal en ce qui concerne l'analyse de sa structure à l'aide de la technique de DN. En outre, le choix du PIB est historiquement pertinent, car Flory a publié des données relatives à ce polymère pour démontrer son hypothèse d'idéalité.

Nous avons simulé le PIB à l'aide d'un modèle existant dans lequel les atomes d'hydrogène ne sont pas représentés explicitement, mais regroupés avec leurs atomes de carbone respectifs afin de former des amas d'atomes unifiés (AU). Une molécule PIB représentée sous forme d'AU est illustrée dans la figure 1.1. Même simplifiée, la structure monomère des atomes unifiés est complexe et les simulations prennent du temps. Il est nécessaire de rassembler de nombreuses données relatives aux chaînes longues, afin d'observer les déviations ; cependant, le temps nécessaire aux simulations de chaînes longues augmente significativement pour les modèles de polymères plus complexes. Les modèles à gros grains, tels les modèles à billes et ressorts (BR), manquent d'informations chimiques et, par conséquent, il est plus aisé d'équilibrer et d'acquérir un nombre raisonnable de configurations de chaînes indépendantes.
Nous avons commencé par simuler un modèle BR, doté d'une rigidité similaire à celle du PIB ; Nous avons développé des algorithmes pour ajouter progressivement des informations atomistiques, selon un modèle à « grains fins » (cf. figure 1.2). Cette méthode nous a permis d' engendrer un grand nombre de configurations de chaînes.

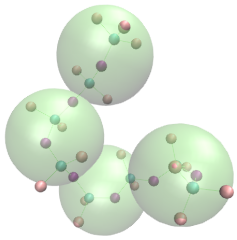

Figure 1.2: Les grandes sphères vertes représentent le modèle à gros grains, dans lequel nous avons introduit les informations atomistiques du PIB.

Déviations de l'hypothèse d'idéalité

Ainsi que nous l'avons expliqué précédemment, de récentes études ont démontré l'existence d'une déviation de la structure des chaîne de polymère par rapport à la pelote gaussienne. Les interactions de très courte portée, résultant de l'incompressibilité du fondu, peuvent agir entre monomères distants le long du contour ce qui entraîne un gonflement de la chaîne. L'effet de ces interactions peut être observé dans le cadre de la fonction de corrélation d'orientation des liaisons ainsi que du facteur de forme.

Fonction de corrélation d'orientation des liaisons

La fonction de corrélation d'orientation des liaisons mesure la façon dont les informations sur la conformation locale décroissent le long de la chaîne principale. En cas d'absence d'interactions de longue portée le long du contour, la fonction de corrélation doit diminuer de façon exponentielle. La figure 1.3 illustre un comportement en loi de puissance, dans la dernière partie de la fonction de corrélation. L'exposant de la loi de puissance équivaut à $-\frac{3}{2}$, conformément à la non-idéalité prévue. Le ralentissement de la décroissance des informations résulte des interactions entre monomères distants le long du contour. Afin d'exclure les effets de bout de chaîne, il est essentiel d'étudier des polymères de longueur suffisante ; de plus, il est nécessaire de calculer la moyenne de la fonction de corrélation d'orientation des liaisons en se basant sur un grand nombre de configurations de chaîne, afin de pouvoir détecter un signal clair.

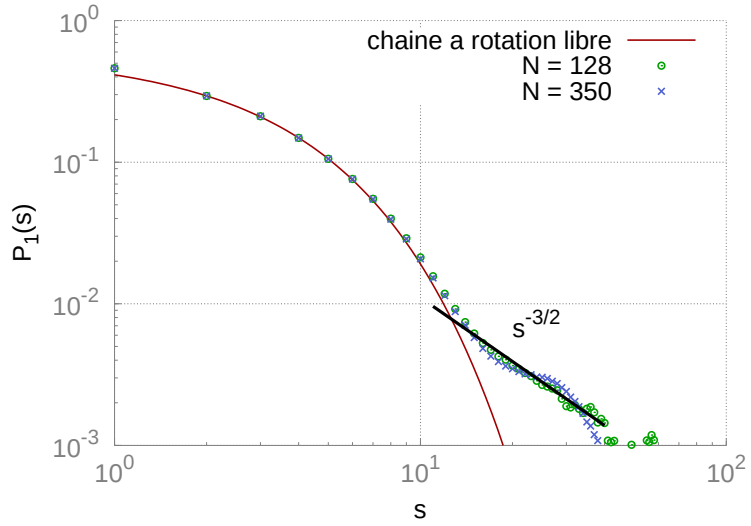

Figure 1.3: Fonction de corrélation d'orientation des liaisons. s représente le nombre de liaisons séparant les segments ; la ligne rouge représente la décroissance exponentielle des chaîmes idéales et la ligne noire indique la loi de puissance.

Facteur de forme

Il est absolument nécessaire de comparer nos simulations avec des données expérimentales. Pour ce faire, nos collaborateurs à Knoxville, aux États-Unis (Tennessee), ont rassemblé des données résultant de la diffusion des neutrons aux petits angles (DNPA) sur un PIB. Jusqu'à présent, les données DNPA soumises aux méthodes d'analyse usuelles ne se sont pas avérées concluantes. Les simulations offrent l'occasion incomparable non seulement d'analyser les données en espace réel, mais également d'utiliser les mêmes configurations de chaîne pour calculer le facteur de forme. Nous sommes en mesure de calculer le facteur de structure d'après les simulations ; cependant, il se peut que le modèle AU, adapté aux simulations, ait un facteur de structure différent. En ajoutant des atomes d'hydrogène explicites au modèle AU, le facteur de structure simulé peut être directement comparé aux données résultant de l'expérience. Cela nous aidera à mieux comprendre comment la diffusion est affectée par les effets de non-idéalité. Nous espérons que le passage de l'espace réel à l'espace réciproque permettra de démontrer la non-idéalité des chaînes polymères.

2 | Introduction

A cornerstone of modern polymer physics is Flory's famous "ideality hypothesis" which states that a chain in a melt behaves as if all intra-chain excluded volume interactions were absent [1–3]. It is generally accepted that any local conformational information (i.e. bond angles or torsional angles) decays exponentially along the chain backbone and thus has no influence on the long range conformation. However, recent theoretical [4, 5] and computational [5–9] results for models of long and flexible polymer chains indicate that there exist deviations from ideal behavior. These deviations stem from the incompressability of the melt which leads to an incomplete screening of the excluded volume interactions by the surrounding chains. The non-ideality of the chains impacts the conformational properties of polymer melts on intermediate length scales. Static quantities such as the bond-bond orientational correlation function, the pair distribution function and its Fourier transform, the form factor, show deviations from the ideal chain hypothesis.

The non-ideality of polymer chains has been extensively studied by means of highly flexible coarse-grained models, such as the bond fluctuation model (BFM) and bead spring model (BS). The results from the coarse grained simulations concur with the analytically predicted deviations [5–9]. These models are so close to the idealized chain (highly flexible and the units (beads) are point-like), that deviations from ideality caused by residual excluded volume interaction are easily identified as such. Real polymers, on the other hand, have a non-negligible stiffness and monomer cross-section. These finite size effects skew the chain properties so that they can no longer be approximated by idealized chain models, which in turn makes it more delicate to differentiate the effects of the residual excluded volume.

To this date residual excluded volume effects have not been experimentally investigated. The work at hand attempts to bridge the gap between coarse-grained simulations and experimental data by implementing an atomistically realistic polymer model. To differentiate between effects caused by chain stiffness and monomer cross-section, and those caused by the incomplete excluded volume screening we additionally employ a chain model that neglects all excluded volume effects, namely the rotational isomeric state model [3]. The insight - gained from the simulations - on how the residual excluded volume affects the structure of real chains can then be directly applied to the analysis of experimental data.

We had to choose one exemplary polymer for this study and the

choice fell on Polyisobutylene (PIB) CH_3-[4C8H]$_N$-H for a number of reasons. It is a polymer whose conformational and dynamic properties have been exhaustively studied both experimentally [10–33] and theoretically [28, 34–40]. For our purposes it is important that the polymer is flexible and has no electrostatic interactions as this would slow down the simulations considerably. We implemented a recently published united atom model of PIB by Tsolou et al. [40], which reproduces the static and dynamic quantities of PIB extremely well.

The presented work focuses on a specific polymer, however we feel that the potential is much broader. Revealing the corrections to chain ideality for PIB should lend confidence to the possibility to detect these universal corrections also in other polymers, thereby stimulating further research in this field, not only for homopolymers but also for polymer blends [41] or polymers in confined geometry (films [42, 43] or pores [44]) where the corrections are predicted to be much larger than in the three-dimensional bulk [4, 43].

The computational challenge of this work is to simulate very long PIB chains. This is necessary to distinguish the effects of chain stiffness and cross-section from the effects of non-ideality. We work with the united-atom (UA) model introduced by Tsolou et al. [40]. Explicit hydrogen atoms do not influence the chain structure and the eight additional particles per monomer would only slow down the simulation. In chapter 3 the UA model is thoroughly discussed and the chain and melt properties analyzed.

In chapter 4 we introduce the computational methods used to tackle the challenge of equilibrating systems consisting of chains of up to $N = 350$ monomers — over four times longer than what has been simulated up to this date. In the same chapter we discuss how we added the explicit hydrogen atoms to our UA model in an effort to correctly reproduce the structure factor as it is measured in small angle neutron scattering experiments (SANS). The final computational method we introduce is the Rotational Isomeric State Monte Carlo "RIS-MC" model. This model is true to chemical detail, but neglects excluded volume interactions, making it a valuable counterpart to the molecular dynamics simulations.

To set the simulations into experimental context, SANS measurements of PIB were performed by our collaborator, and analyzed in the scope of this thesis. Chapter 5 details the challenges of interpreting the SANS data and the comparison to the simulation.

The result of this work is discussed in chapter 6, where we analyze the simulation data in the light of non-ideality effects and attempt to do the same with the experimental data comparing both to theoretical predictions.

Flory's ideality hypothesis is manifested in the 1983 publication by Hayashi et al. [17] which shows that the RIS predictions and the SANS data concur. By reproducing the RIS model according to Vacatello and Yoon [39] and evaluating the effect of polydispersity on the scattering picture we are able to shed a new light onto the past results.

An overview of the results of this thesis and an outlook onto future

projects is given in the final chapter 8.

3 | System characteristics

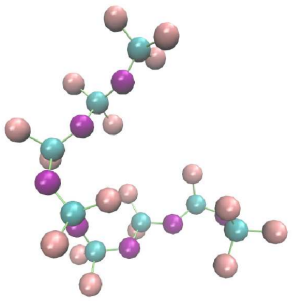

Figure 3.1: A short PIB chain in united atom (UA) representation. The bead colors refer to different UA sites: The methyl groups are orange, the methylene groups are purple and the quaternary C atoms are turquoise. The bead sizes are not to scale.

Tsolou et al. [40] recently presented a molecular dynamics (MD) simulation of the sorption of small gases in Polyisobutylene (PIB). To this end it was necessary to construct a simulation model of PIB that correctly reflects its microscopic and macroscopic quantities. Although there have previously been UA models of PIB presented in the literature, some quantities such as the dihedral distribution were not correctly described [16, 45]. The force fields proposed by Tsolou et al. correctly represent the splitting of the rotational states and the resulting chain stiffness. The macroscopic values such as the chain length dependence of the density coincide with experimental results. This is why we decided to implement the united atom model of PIB introduced by Tsolou. The following chapter presents our extensive analysis of the PIB systems simulated by applying the force fields proposed by Tsolou et. al.

All simulations are performed with the molecular dynamics simulator LAMMPS (9 January 2009 version) [46]. The systems that are studied in the scope of this work are simulated at higher temperatures and consist of longer chains than those published by Tsolou et al. Hence it has to be verified that the force fields are stable under these conditions. The following chapter successively introduces the monomer, chain and melt properties.

3.1 The monomers

In the united atom (UA) model of PIB that we use the hydrogen atoms are not explicit, but grouped together with their respective carbon atoms. This leads to a monomer consisting of four UA beads, namely one carbon bead, one methylene bead and two methyl beads. The end groups are composed of one carbon bead and three methyl beads. Thus, a chain with N monomers consists of $(4N+1)$ UA beads. A visualisation of a short PIB chain in UA representation is shown in fig. 3.1.

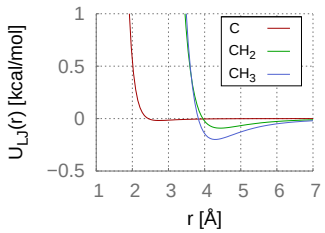

Figure 3.2: Above the LJ interaction potentials of the three UA sites in comparison. The UA bead representing the methyl group has the largest excluded volume.

Non-bonded interaction

The size of the UA beads depends on how many hydrogen atoms are grouped together and varies from carbon being the smallest to the methyl groups (CH_3) being the largest, see fig. 3.2. The excluded volume interaction between two beads i and j separated by the distance

r_{ij} is defined by a 6-12 Lennard-Jones (LJ) potential

$$U_{\mathrm{LJ}}(r_{ij}) = 4\epsilon_{ij}\left[\left(\frac{\sigma_{ij}}{r_{ij}}\right)^{12} - \left(\frac{\sigma_{ij}}{r_{ij}}\right)^{6}\right]. \tag{3.1}$$

The values for the σ_{ij} and ϵ_{ij} are calculated by the Lorentz-Berthelot combining rule [47, 48] which uses the geometric average for ϵ and the arithmetic average for σ

$$\sigma_{ij} = \frac{1}{2}(\sigma_i + \sigma_j) \quad , \qquad \epsilon_{ij} = \sqrt{\epsilon_i \epsilon_j}. \tag{3.2}$$

The values for the parameters ϵ_i and σ_i can be found in table 3.1 at the end of this chapter. The LJ interaction is set to zero for interaction pairs that are separated by more then 12Å, so that $r_{\mathrm{cutoff}} = 12$Å. It is not necessary to apply a shift factor to the potential since $U_{\mathrm{LJ}}(r_{\mathrm{cutoff}}) < -10^{-4}$kcal/mol.

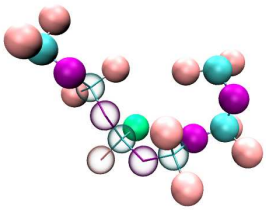

Figure 3.3: Here a chain segment from the view point of the green colored methyl group is depicted. The transparent beads are invisible to the methyl group while the solid colored beads interact fully with the marked methyl group. The beads are not to scale.

The bead diameters are between 2Å–3.5Åwhich makes the beads larger then the bonds ($l = 1.54$Å) connecting them. This causes the excluded volume of neighbouring beads along the chain to strongly overlap, giving rise to very large forces. To circumvent this problem beads along a chain only interact with one another if they are separated by four or more bonds see fig. 3.3 in the margin. Since the side groups of neighbouring monomers are separated by four bonds they fully interact which leads to the preference of the gauche and trans rotational states. The regulation of the interaction potentials of close neighbours along the chain is referred to as "special bonds" inside LAMMPS.

Bonded interaction

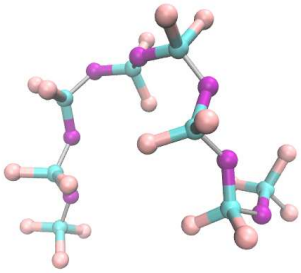

Figure 3.4: In this figure the bonds regulated by SHAKE are drawn with thick lines while the bonds regulated with the harmonic potential are drawn by thin grey lines.

Chemical bonds are very stiff and the bond length fluctuations are small (≈ 0.005Å) [2, p. 49]. It is challenging to emulate the stiffness of chemical bonds. To this end Tsolou et al. propose the use of the SHAKE algorithm [49]. At each time step the bonds regulated via SHAKE are set back to their equilibrium length by applying an additional constraint force. SHAKE adjusts the bond-length until it is within the tolerated bounds, or the maximum number of iterations is reached, whichever event occurs first. We choose the tolerance to be $\delta = 0.001$Å and the maximal number of iterations is set to 30. To guarantee for good parallel processing, LAMMPS only allows for small clusters to be constrained via SHAKE. In our case the bonds inside a monomer are regulated by SHAKE (CH_2–C, C–CH_3) while the bond connecting two monomers (C–CH_2) is defined by a harmonic potential

$$U_{\mathrm{bond}}(l) = K(l - l_0)^2 \tag{3.3}$$

with a strong spring constant K the value of which is noted in table 3.1. Fig. 3.4 visualises the arrangement of the different bond types in a chain. The harmonic bonds are represented by the thin grey lines while the SHAKE regulated bonds are thicker.

Since some simulations are performed at very high temperatures, the stability of the SHAKE algorithm must be tested. The plot on the left of

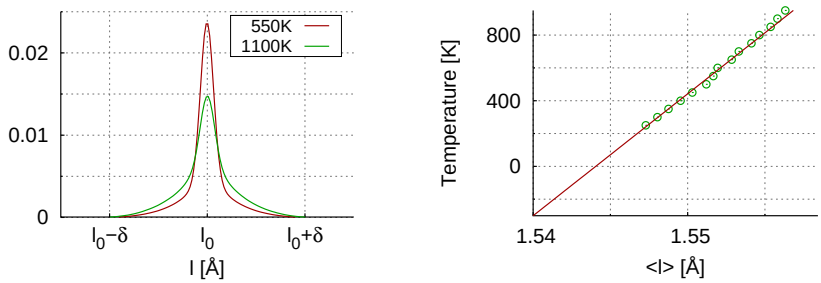

Figure 3.5: The images above show the temperature dependency of the bonds. The left-hand-side shows the bond-length distribution for the bonds regulated with the SHAKE algorithm. The equilibrium length l_0 is 1.54Å and the tolerance $\delta = 0.001$Å. With rising temperature the distribution becomes wider, but does not exceed the tolerance. Even for temperatures as high as 1100K the SHAKE algorithm is stable. The plot to the right shows the mean bond-length of the harmonic bond at varying temperature. The red line is a guide to the eye and shows that a bond-length of 1.54Å would be reached at the fictitious temperature of $-300K$, if the dependence would continue to be linear at even lower temperatures.

fig. 3.5 compares the bond-length distribution at different temperatures. Though the distribution becomes wider with rising temperature, the mean bond-length does not drift and the distribution does not exceed $l_0+\delta$. This proves that even at very high temperatures, here 1100K, the SHAKE algorithm is reliable. For the harmonic bond the equilibrium value of $l_0 = 1.50$Å is suggested. Tsolou et al. argue that due to the steric repulsion of the methyl groups the bond will stretch and its resulting mean value will be equal to that of the SHAKE bonds. Our analysis shows that the bond is stretched even further, exceeding 1.54Å at all temperatures. On the right in fig. 3.5 the temperature dependence of the mean harmonic bond length is plotted. The extrapolation to low temperatures indicates that a bond length of 1.54Å cannot be reached under normal circumstances. Most simulations were performed at 550K. At this temperature the harmonic bond has a mean length of 1.552Å and is 0.012Å longer than the SHAKE controlled bonds. The deviation is less than 1%, so we continued with the suggested parameters.

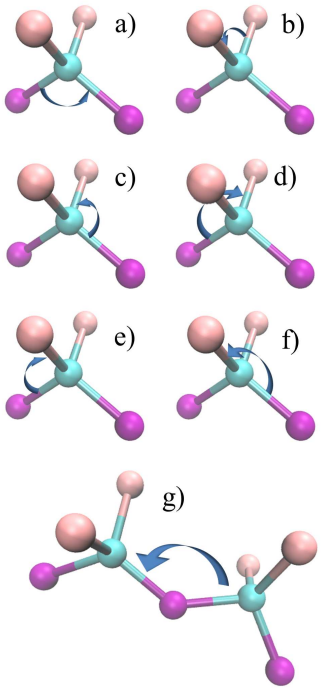

Figure 3.6: The panels above are to help visualise the seven applied angle potential. All angles a) through f) are set to the tetrahedral value, while the backbone angle g) is wider.

Angle potentials

The angles defining the architecture of the PIB monomer have been studied by x-ray scattering [50]. The results show that the angles inside the monomer are dihedral angles of 109.47° (angles a)-f) in fig. 3.6) and the interdiad backbone angle (angle g) in fig. 3.6) has a mean value of 128°. To construct the monomer six angle potentials must be applied to each monomer and an additional angle potential regulates the backbone angle connecting two monomers. All seven angles, a) through g), are shown in fig. 3.6. They are regulated by a harmonic bending potential

$$U_{\text{angle}}(\theta) = K_\theta(\theta - \theta_0)^2 \tag{3.4}$$

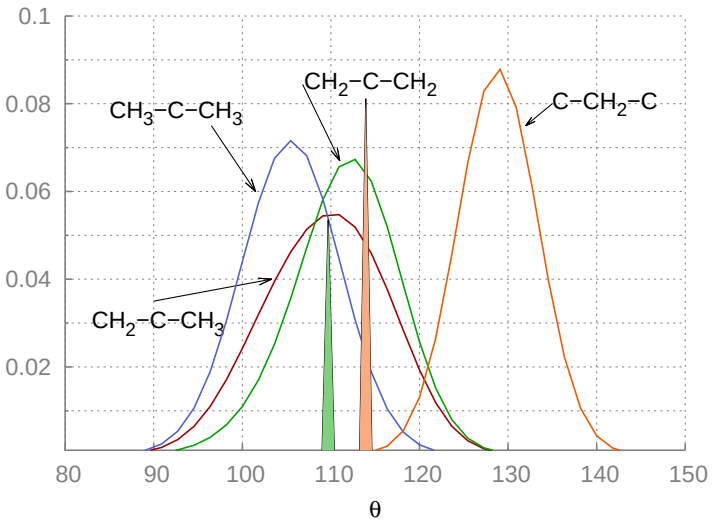

Figure 3.7: The angle distributions are distorted from their equilibrium values 109.5° and 114° due to the excluded volume interaction of the beads. The mean values of the backbone angles are $\theta^{\mathrm{a}} = 112°$ and $\theta^{\mathrm{g}} = 129°$ at 550K. The filled curves are the expected distributions for the tetrahedral angle (green) and the interdiad angle (orange). They are calculated with $\exp\left(-U_\theta/k_{\mathrm{B}}T\right)$ and for reasons of legibility not drawn to scale.

where the bending constant K_θ is the same for each angle and can be found together with the equilibrium values θ_0 in table 3.1. As with the bonds the excluded volume interaction of the UA beads interferes with the applied potentials which leads to the mean angle widths being distorted from their chosen equilibrium values. All angles inside the monomer, connecting the methyl and methylene groups with the quaternary C atom, are set to the tetrahedral angle $\theta_0^{\text{a-f}} = 109.47°$ while the bond angle between two monomers is set to the equilibrium value of $\theta_0^{\mathrm{g}} = 114°$. Methyl crowding stretches the backbone bond angles θ^{a} and θ^{g} further so that their mean values at 550K are 112° and 129°, respectively. Fig. 3.7 shows the distribution of all angles to visualise the distortion from the equilibrium values. Tsolou et al. published the value of $\theta^{\mathrm{a}} = 110°$ which contradicts our findings. For the average over all tetrahedral angles $\theta^{\text{a-f}}$ however we find 109° which leads to the assumption that Tsolou et al. calculated the mean over all six dihedral angles $\theta^{\text{a)-f)}}$ as opposed to only the intradiad back-bone angles θ^{a}. Though the mean angle widths slightly stray from the values found experimentally, it is not expected that this gravely influences the global chain structure.

Torsional potential

The probability distribution of the torsional backbone angles (ϕ) is of great importance to the structure and influences such key quantities as the chain stiffness. Section 4.3 discusses the torsional distribution in great detail. The backbone dihedral has two preferred states, the gauche

and the trans state. We further distinguish between gauche plus and gauche minus to display the dihedral distribution in full 360° mode. At close inspection a splitting of these states becomes apparent so that the dihedral distribution has 6 preferred states. This will be discussed in detail in segment 4.3. The origin of this splitting is the steric repulsion between neighboring methyl groups. In the PIB model at hand, methyl group crowding alone, i.e. the LJ interaction between methyl groups of neighboring monomers, leads to a torsional distribution with distinctive gauche and trans states. Nevertheless, a dihedral potential is applied to the backbone bonds to fine-tune the torsional states. Fig. 3.8 illustrates the differences between the dihedral distribution that originates solely from methyl group crowding and the one being aided by an additional dihedral potential. The harmonic dihedral potential used is given by

$$U_{\text{dihedral}}(\phi) = K_\phi(1 + \cos(3\phi)), \tag{3.5}$$

the value of the bending constant K_ϕ can be found in table 3.1.

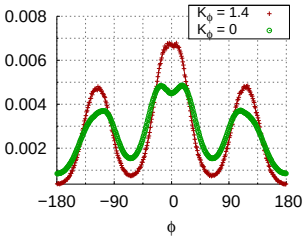

Figure 3.8: Torsional distribution function at 550K. The nonbonded interaction between the methyl groups of two neighbouring monomers gives rise to a threefold torsional distribution. Tsolou et al. suggest adding an additional dihedral potential to the system to amplify the effect.

3.2 Total chain characteristics

After reviewing the potentials which give rise to the architecture of the monomers this section discusses the chains that result once the monomers are strung together.

A very simple polymer model is the freely jointed chain (FJC) where every segment is linked to the previous one by randomly choosing a direction. This chain then resembles a random coil and the average size of the chain is described by the equation

$$R_{\text{ee}} = \sqrt{\langle R_{\text{ee}}^2 \rangle} = a\sqrt{N} \tag{3.6}$$

where R_{ee} is the length of the end-to-end vector, a is the segment length and N the number of segments. From textbooks [2, 51] it is expected that any flexible polymer chain of sufficient length and without any long-range inter-monomer interactions can be described on large scales by the FJC model. As a first approach we follow this classical idea and compare it to our PIB model. It is only necessary to choose the segment length large enough so that the chemical structure of the polymer is lost in the coarser grain. Other than that the choice of scaling is arbitrary because of the self-similar nature of polymer coils. That is, a chain with N segments of length a can be rescaled by λ so that it has $N' = N/\lambda$ segments of length $a' = a\sqrt{\lambda}$. The idea of the scaling argument is, that the global properties are independent of the local, or molecular, structure and are hence invariant under the transformation. The equation

$$R_{\text{ee}} = a\sqrt{N} = a'\sqrt{N'} \tag{3.7}$$

holds for any λ for which $1 \ll N'$ and $l_{\text{p}} \ll a'$ where l_{p} is the persistence length, see eq. (3.13).

Polyisobutylene is a real polymer with bending and rotational potentials that lead to stiffness. Eq. (3.6) still holds for large N but the segment length a must be replaced by the statistical segment length a_0. Fitting

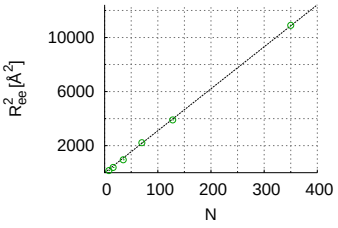

Figure 3.9: The square end-to-end distance R_{ee} of PIB chains of different length N at 550K. The data are fitted with eq. (3.6) and yield a value of $a_0 = 5.57$Å for the statistical segment length.

eq. (3.6) to the data in fig. 3.9 returns a value of $a_0 = 5.57$Å. The statistical segment length is larger for less flexible chains. A more widely spread measure for the chain stiffness is Flory's characteristic ratio C_∞ [51, p. 27]. For chains with n backbone bonds of average square length $\langle l^2 \rangle$ the end-to-end distance is

$$R_{\mathrm{ee}}^2(n) = C_n 2(N-1)\langle l^2 \rangle \tag{3.8}$$

$$= C_\infty 2N\langle l^2 \rangle \qquad \text{for } N \to \infty, \tag{3.9}$$

for two backbone bonds per monomer as in the case of PIB. The average square bond-length in our model is $\langle l^2 \rangle = 2.3718\text{Å}^2$ and comparing eq. (3.6) and eq. (3.9) leads to $C_\infty = a_0^2/2\langle l^2 \rangle = 6.53$.
Another method to choose the segment length is to make sure that not only the size, but also the contour length of the polymer chain and its FJC equivalent are equal. A FJC that fulfils these conditions is called a Kuhn chain and its segment length is denoted by a_{K} and the number of Kuhn-segments is N_{K} [2, p. 54]. The contour length $R_{\max}$ is

$$R_{\max} = a_{\mathrm{b}} N = a_{\mathrm{K}} N_{\mathrm{K}} \tag{3.10}$$

with a_{b} the length of a monomer. We chose to measure the monomer length as the distance between two quartenary carbon beads. Though it might seem more intuitive to define the distance between two methylene groups as the monomer length, we chose the aforementioned distance because much of our analysis is done regarding solely the quartenary carbon beads. This distance can be calculated to $a_{\mathrm{b}} = 2l\sin(\theta^{\mathrm{g}}/2) = 2.77$Å, though an analysis of the simulation data results in a slightly larger value $\langle a_{\mathrm{b}} \rangle = 2.788$Å. It is possible to compute the length of a Kuhn-segment by comparing coil size and contour length as follows

$$R_{\mathrm{ee}}^2 = a_0^2 N = a_{\mathrm{K}}^2 N_{\mathrm{K}}, \quad a_{\mathrm{K}} = \frac{R_{\mathrm{ee}}^2}{R_{\max}}. \tag{3.11}$$

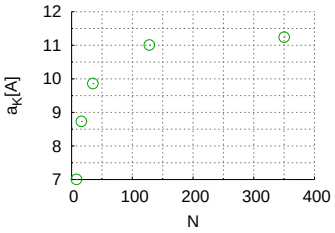

Figure 3.10: Kuhn segment length calculated from eq. (3.11) for different chain lengths N. For shorter chains the chain-end-effects cause a_{K} to be smaller, but it approaches a value of $a_{\mathrm{K}} = 11.25$Å for long chains.

Fig. 3.10 shows the Kuhn-segment length for different chain lengths at 550K. Though a_{K} should be independent of N, chain-end-effects dominate the shorter chains. For longer chains the value of a_{K} approaches $a_{\mathrm{K}} = 11.25$Å.
A related quantity to measure the chain stiffness is the persistence length l_{p}. It tells us when the bond-bond correlation function K_{bb} has decorrelated. Let the unit vectors of the bonds be $\hat{b}_i$, then the bond-bond correlation function is

$$K_{\mathrm{bb}}(|i-j|) = \langle \hat{b}_i \cdot \hat{b}_j \rangle \tag{3.12}$$

and the persistence length l_{p} is

$$l_{\mathrm{p}} = a \sum_{i=0}^{\infty} \langle \hat{b}_i \cdot \hat{b}_{i+1} \rangle. \tag{3.13}$$

For a FJC all bonds are decorrelated and $\langle \hat{b}_i \cdot \hat{b}_j \rangle = 0$ for all $i \neq j$. At this point it is advisable to introduce a chain model that takes bending

stiffness into account. In the freely rotating chain (FRC) model the bonds are linked together forming an angle θ while the rotational angle is chosen freely. The correlation function for a FRC is

$$K_{\mathrm{bb}}(|i-j|) = \langle \hat{b}_i \cdot \hat{b}_j \rangle = (\cos(\pi - \theta))^{|i-j|}. \tag{3.14}$$

At this point it is beneficial to move to a continuum picture of the chain where the integer $|i-j|$ becomes s and $K_{\mathrm{bb}}(|i-j|) = P_1(s)$. As discussed in more detail in [2, p. 56] the correlation decays very quickly along the backbone and can be approximated by

$$P_1(s) = \langle \cos(\pi - \theta) \rangle \, \mathrm{e}^{-s/s_{\mathrm{p}}} \tag{3.15}$$

with s_{p} the number of segments per persistence length which makes $l_{\mathrm{p}} = \langle a_{\mathrm{b}} \rangle \langle \cos(\pi - \theta) \rangle s_{\mathrm{p}}$ with $\langle a_{\mathrm{b}} \rangle$ the mean distance between two quartenary carbon atoms. Fig. 3.11 shows the bond-bond correlation function between the quartenary carbon UA cites. From this plot we extract a value of $s_{\mathrm{p}} = 2.929$ and $\langle \cos(\pi - \theta) \rangle = 0.581981$ by fitting eq. (3.15) to the data of the longest chains. This results in a persistence length $l_{\mathrm{p}} = 4.75$Å with the mean C–C distance $\langle a_{\mathrm{b}} \rangle = 2.788$Å.

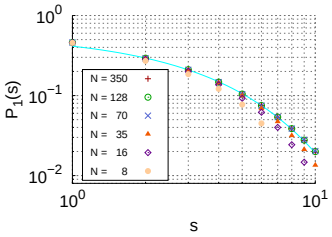

Figure 3.11: The bond-bond correlation function P_1 for chains of different lengths is shown. While the shorter chains ($N = 8$, 16) are dominated by chain-end effects, the longer chains show the typical exponential decay. s is the monomer number, the correlation function is measured from quartenary carbon bead to quartenary carbon bead.

We have calculated the properties of the PIB chains by applying very simple models that neglect all types of long-range interactions. We are interested in how well these parameters describe the internal structure of the coil. To this end we compare the internal distance function $R^2(s)$ of a FRC with the data of the simulated PIB chains. For a FJC with $\vec{r}$ denoting the bond vectors of length a the internal distances function is

$$R^2(s) = \sum_{i=1}^{s} \sum_{j=1}^{s} \langle \vec{r}_i \cdot \vec{r}_j \rangle = sa^2 \tag{3.16}$$

which leads to eq. (3.6) for $s = N$. For the FRC the correlation between bonds must be taken into account which leads to

$$\frac{R^2(s)}{s} = \langle a_{\mathrm{b}}^2 \rangle + \frac{2\langle a_{\mathrm{b}}^2 \rangle \langle \cos\theta \rangle}{s} \frac{\mathrm{e}^{-\frac{1}{s_{\mathrm{p}}}}}{[1 - \mathrm{e}^{-\frac{1}{s_{\mathrm{p}}}}]^2} \left(s(1 - \mathrm{e}^{-\frac{1}{s_{\mathrm{p}}}}) - (1 - \mathrm{e}^{-\frac{s}{s_{\mathrm{p}}}}) \right) \tag{3.17}$$

as detailed in [2, p. 56-59]. In fig. 3.12 the simulation data is shown together with eq. (3.17). The dashed line shows eq. (3.17) with the following parameters: The value of $\langle a_{\mathrm{b}}^2 \rangle = 7.758\text{Å}^2$ that was taken from the analysis of the distance distribution, $\langle \cos\theta \rangle = -0.58198$ and $s_{\mathrm{p}} = 2.92889$ are the fitted values of eq. (3.15). Fig. 3.12 shows that this curve underestimates the internal distances and leads to a smaller chain stiffness. The solid curve shows a fit of eq. (3.17) to the data of the longest chain where monomer length a_{b} is the fit parameter. A FRC with longer monomers, namely $a_{\mathrm{b}} = 2.84$Å describes the collected data rather well.

3.3 Melt characteristics

If not indicated otherwise all simulations are conducted under constant temperature and pressure. The temperature is controlled by a Nosé-Hoover thermostat and the pressure is regulated by a Nosé-Andersen

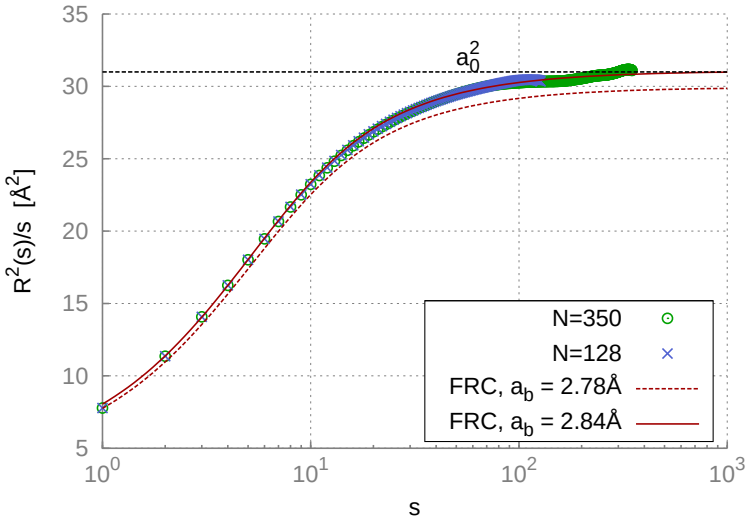

Figure 3.12: The intra chain distances with the fit of eq. (3.17) .

barostat. The equations of motion are those published by Shinoda [52] which are propagated by the time integration method introduced by Tuckerman [53] which is a slightly modified Verlet integrator. The integration step length is set to 2 fs if not indicated otherwise. LAMMPS calls for damping parameters of the temperature and pressure. These parameters are in time units and influence how strongly fluctuations from the goal values of temperature and pressure are damped. It is important to choose these parameters with care as to avoid oscillations in the system. The temperature damping constant is $t_{\mathrm{damp}} = 300$fs for all systems and temperatures. The pressure damping constant p_{damp} was chosen depending on the size and density of the system by

Lammps sample code:
```
fix all npt temp 550.0
550.0 300.0 iso 0.9869
0.9869 20000.0
```

$$p_{\mathrm{damp}} = \frac{3}{2\pi}\frac{M^{5/6}}{\sqrt{k_{\mathrm{B}}T}}\left(\nu n_{\mathrm{atoms}}\right)^{1/3} \tag{3.18}$$

where $M = 23.3 \times 10^{-27}$kg is the average mass per UA bead, k_{B} is the Boltzmann constant, T is the temperature, n_{atoms} is the total number of UA beads in the System and ν is the specific volume of the system.In all performed simulations the pressure is set to 1 atm.

3.3.1 Static quantities

Given the nature of their research Tsolou et al. had to pay special attention that the density of the PIB melt is correctly reflected by the simulation. The density of polymer melts varies with chain length and temperature.
The end groups of polymer chains occupy a larger volume than intra-chain monomers that are flanked by neighbouring groups at each side. A melt that consist of short chains accommodates more chain-ends per unit volume then a melt of longer chains. Thus the volume is larger in the melt of short chains and the density is lower. The chain length

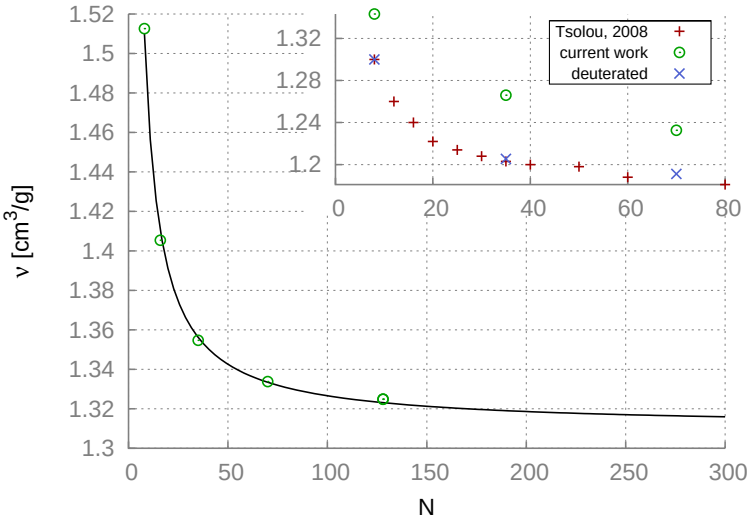

Figure 3.13: The specific volume ν is dependent on the chain length. The plot shows ν for different chain length at 550K. The line is the fit of eq. (3.19) to our data. Inset: To compare with Tsolous data we evaluated the specific volume at 450K and notice that our data is off set to larger values compared to that presented by Tsolou. When the calculation is done for deuterated PIB our data coincides with that of Tsolou.

dependence of the specific volume ν is described by

$$\nu = \nu_\infty + \frac{\nu_0}{N} \tag{3.19}$$

with ν_∞ being the limit for very large chains [31]. A fit of eq. (3.19) to our data produces $\nu_\infty = 1.31\text{cm}^3/\text{g}$ and $\nu_0 = 1.60\text{cm}^3/\text{g}$. Tsolou et al. conducted the bulk of their simulations at $T = 450\text{K}$, so to compare with their findings we also simulated three systems at 450K. Though the shape of the curve is the same as that published by Tsolou, our data is off set to a higher specific volume. Flabbergasted as to why this might be, we finally came to the conclusion that Tsolou et al. did their volume calculations for deuterated polymers (CD_3–$[C_4D_8]_N$–D), whereas we calculated the mass of the polymers with hydrogen (CH_3–$[C_4H_8]_N$–H). If we recalculate the specific volume replacing the mass of hydrogen with that of deuterium, our data coincides with that of Tsolou et al., see fig. 3.13. Polymer melts expand with rising temperature, so the specific volume is also temperature dependent. There are different empirical equations to describe the temperature dependence of ν. Eichinger and Flory [54] use the following equation to analyse their work

$$\nu_\infty^{\text{Flory}}(T) = (0.9297 - 5.123 \cdot 10^{-4}(T - 273) + 6.15 \cdot 10^{-8}(T - 273)^2)^{-1}. \tag{3.20}$$

Fetters et al. [31] proposed another empirical equation

$$\nu_\infty^{\text{Fetters}}(T) = 1.077 + 6.8 \cdot 10^{-4}(T - 273). \tag{3.21}$$

In fig. 3.14 both equations are compared to the data of a melt of chains with $N = 128$. At low temperatures, between 250K and 450K, the

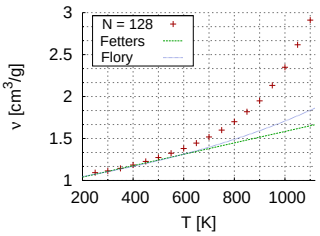

Figure 3.14: The specific volume of a polymer melt with $N = 128$ is studies at different temperatures and compared to predictions made by comparison to experimental data. At low temperatures the Fetters equation fits well, at higher temperatures the specific volume becomes very large.

behavior of the specific volume is described well by both eq. (3.20) and eq. (3.21) At temperatures above 500K our data deviates from the predictions towards higher values of ν. Eq. (3.20) and eq. (3.21) are empirical equations to describe experimental data. A real melt would disintegrate at temperature as high as 1100K. Hence it is to be expected that the simulation data do not follow the predictions at extreme temperatures.

The compressability is the quantity which describes the relative ease with which condensed matter can be compressed. The isothermal compressability can be derived from the volume fluctuations as is explained in [51] by

$$\begin{aligned}\kappa_{\mathrm{T}} &= -\frac{1}{V}\frac{\partial V}{\partial p}\bigg|_{\mathrm{T}} \\ &= \frac{1}{V}\frac{1}{k_{\mathrm{B}}T}\langle \delta V^2\rangle_{\mathrm{npt}} \\ &= \frac{1}{V}\frac{1}{k_{\mathrm{B}}T}(\langle V^2\rangle - \langle V\rangle^2)\end{aligned} \tag{3.22}$$

with k_{B} the Boltzmann constant, V the volume and p the pressure. Fig. 3.15 shows the temperature dependence of κ_{T} for different chain lengths. It is notable that the compressablity is higher for shorter chains. It is likely that the lower density is cause of this effect.

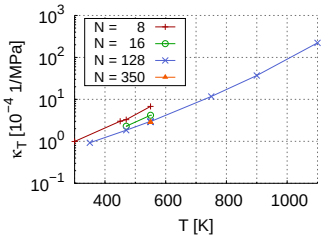

Figure 3.15: The temperature dependence of the compressability for chains of different degrees of polymerisation is shown above.

3.3.2 Dynamical properties

Though the focus of this work is on the static properties of PIB it is important to study the dynamics of the system to see if it propagates regularly and to estimate the relaxation times.

We can roughly divide the time scales on which a polymer chain diffuses into three regions. On very short time scales the atoms, or UA beads in our case, move unhindered in the "free volume" surrounding them. The mean square distance (msd) they travel is much smaller than the size of a monomer. On this time and length scale the movement of the beads is purely ballistic. The position of the beads at time t is denoted by $\vec{R}(t)$ and the mean square displacement is

$$\langle[\vec{R}(0) - \vec{R}(t)]^2\rangle \propto t^2 \tag{3.23}$$

for times $t \ll \tau_0$ and distances smaller than the bead diameter a_{b}. Once the atoms, or beads, move beyond distances of the order of themselves their dynamics slows down due to the connectivity of the chain and frictional forces. The viscoelastic properties can be described by the Rouse model according to the textbook knowledge [1, 2, 51]. Though this model neglects all hydrodynamic interactions as well as excluded volume effects it describes the dynamics of unentangled chains rather well. The Rouse model treats a polymer as a bead-spring chain. The equations of motion can either be derived from the mechanical model or from the Langevin equations as is explained in [1, p. 63]. Either way results in the coupled differential equation

$$\xi\frac{\partial \vec{R}_n}{\partial t} = \frac{3k_{\mathrm{B}}T}{a_{\mathrm{b}}}\frac{\partial \vec{R}_n}{\partial n} + \vec{f}_n \tag{3.24}$$

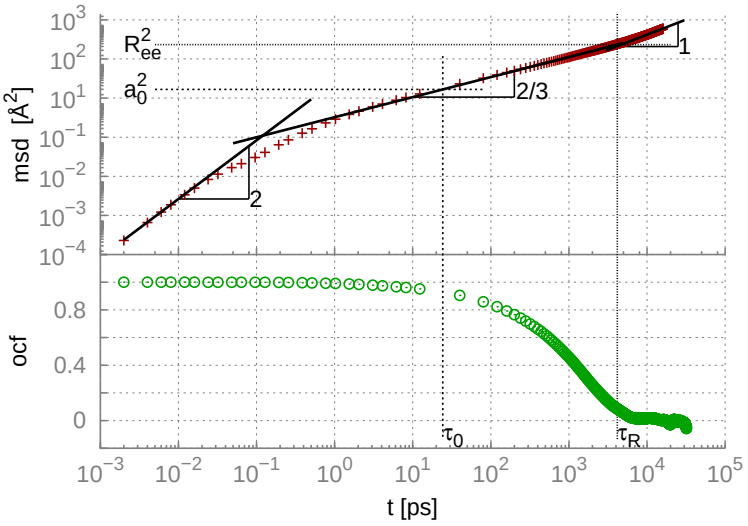

Figure 3.16: The plots above show the dynamics of a melt of 256 chains of length $N = 35$ at 550K. The upper panel shows the mean square displacement of all UA beads constructing the chain. The lower panel shows the orientational correlation function (ocf) of the end-to-end vector. The ocf is sufficiently decorrelated once the chain has diffused by R_{ee}. This time is called the Rouse time τ_{R}.

with ξ the friction coefficient, n the index number of monomers along the chain, and $\vec{f}_n$ the random force of the Langevin equation. To solve eq. (3.24) we follow [1] and use the amplitudes of the vibrational modes, the Rouse modes, $\vec{X}_p$ as generalised coordinates. Via time correlation it is possible to identify the relaxational times τ_p

$$\langle \vec{X}_p(t) \cdot \vec{X}_p(0) \rangle \propto \exp -t/\tau_p, \quad t \gtrsim \tau_0 \tag{3.25}$$

with $\tau_N = \tau_0$ being the time it takes for a single monomer to relax and $\tau_1 = \tau_{\text{R}}$ is called the Rouse time and is the time it take for a chain to diffuse a distance of order R_{ee}. On time scales $\tau_0 \leq t \leq \tau_{\text{R}}$ the chains show viscoelastic properties and the mean square displacement is

$$\langle [\vec{R}(0) - \vec{R}(t)]^2 \rangle \propto t^{1/2}, \quad \tau_0 \ll t \ll \tau_{\text{R}} \tag{3.26}$$

On time scales larger than τ_{R} and distances greater than R_{ee} the motion of the coil is purely diffusive and can be described by Brownian motion.

$$\langle [\vec{R}(0) - \vec{R}(t)]^2 \rangle \propto t, \quad \tau_{\text{R}} \gg t. \tag{3.27}$$

Fig. 3.18 shows the different regimes of diffusive behaviours for a polymer melt and compares the mean square displacement (msd) with the orientational correlation function (ocf) of the end-to-end vector. The plot demonstrates that the chain configurations decorrelate for times $t \gg \tau_{\text{R}}$.

Fig. 3.17 compares the polymer motion in the viscoelastic regime for chains of different lengths. The shorter chains diffuse more quickly which is due to a number of reasons, the lower density and the higher

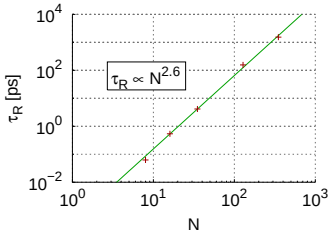

Figure 3.17: The Rouse time depends on the length of the chain, but in our simulation the dynamics is considerably slower then predicted ($\tau_{\text{R}} \propto N^2$ [2]).

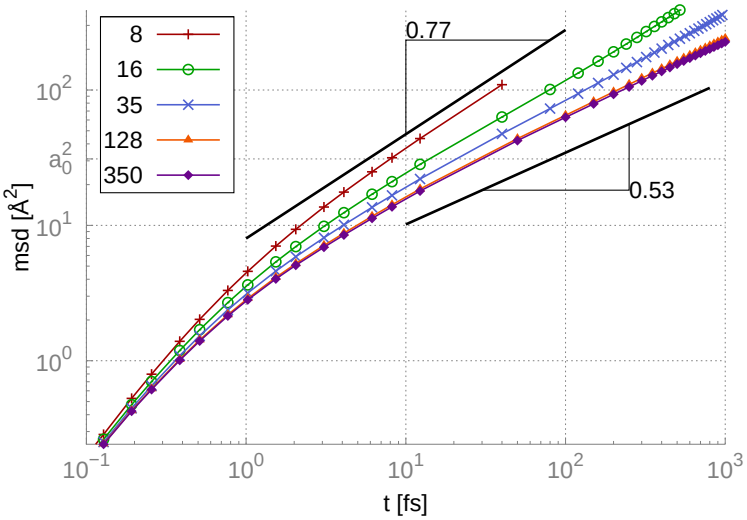

Figure 3.18: The plot compares the msd of all monomers on intermediate timesscales for chains of different length at $T = 550\,\mathrm{K}$. While the earlytime regime is roughly independent of the chain length, the dynamics in the Rouse regime is much faster for shorter chains. For long chains the Rouse dynamics appears to converge towards msd $\propto t^{0.53}$.

mobility of the end groups to name two. For long chains the dynamics converges to msd $\propto t^{0.53}$ which is close to the Rouse model.

In our simulations we want to sample as many independent chain configurations as is feasable. To realize this it is important to estimate the Rouse times of the chains. The Rouse time is predicted to scale with the degree of polymerisation as $\tau_\mathrm{R} \propto N^2$ for an unentangled chain. Fig. 3.17 in the margin shows the relaxation times at 550K for chains of different length. Our dynamics are considerably slower, with a $\tau_\mathrm{R} \propto N^{2.6}$ behavior.

Non-bonded interaction

site	ϵ (kcal/mol)	σ (Å)
C	0.018	2.44
CH_2	0.091	3.95
CH_3	0.199	3.825

Bond potential

bond	K (kcal Å$^{-2}/mol$)	l_0 (Å)
CH_2–C	SHAKE	1.54
C–CH_3	SHAKE	1.54
C–CH_2	192	1.50

Angle potential

angle	K_θ (kcal rad^{-2}/mol)	θ_0 (deg)
CH_3–C–CH_3	62.1	109.47
CH_2–C–CH_3	62.1	109.47
CH_2–C–CH_2	62.1	109.47
C–CH_2–C	62.1	114.00

Torsional potential

dihedral	K_ϕ (kcal/mol)
CH_2–C–CH_2–C	1.4
C–CH_2–C–CH_2	1.4

Table 3.1: These are the interaction parameters suggested by Tsolou et al. for a UA description of PIB. We implemented the force fields unaltered.

4 | Computational Methods

The computational challenge of this work is to generate as many independent polyisobutylene (PIB) chains and gather as much information about the coil structure as possible. In the following an array of computational tools is introduced and discussed. First it is discussed how the problem of the very large relaxation times for the chain lengths under consideration has been alleviated. This is followed by a section on how we added the explicit hydrogen atoms to the united (UA) model of PIB for a more distinguished scattering picture. In the final section the rotational isomeric state (RIS) Monte Carlo method which generates chain configurations based on the torsional probability distribution is discussed.

4.1 System set up and equilibration

The deviation from ideality we wish to observe only becomes apparent for chains of sufficient length, that is onward of a degree of polymerization of $N \geq 100$. When dealing with a more complex polymer model, like polyisobutylene in our case, the simulation time rises significantly with the chain length. To equilibrate a melt consisting of chains with such detail and with the required length proves to be very time consuming. Furthermore for the sake of good statistics sampling many independent chain configurations is essential. To this end we explored a variety of different methods that allow us to produce as many independent chain configurations in as little time as possible. The shorter chains for which the Rouse time is easily reached are set up in an all-trans configuration and equilibrated until the system is isotropic. In a more advanced approach, the chemical details of PIB are neglected for the duration of the equilibration and then added back to the model in a process termed back mapping or fine graining. In an effort to avoid the long relaxation times and produce uncorrelated chain configurations in a smaller amount of time we employed a method termed "temperature runs" in which the systems are intermittently run at very high temperatures and cooled back down.

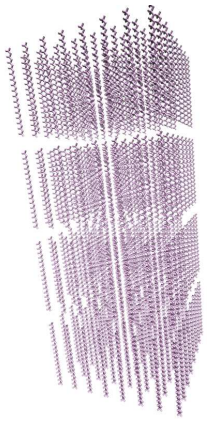

Figure 4.1: The "all-trans" starting configuration of a melt of 256 chains of length $N = 16$. The picture shows clearly that the excluded volumes do not overlap in this method.

4.1.1 All-trans setup

This section describes a very simple method to generate a PIB melt, namely the all-trans setup. "All-trans" refers to the artificial chain configuration in which all back-bone UA beads are in one plane. This

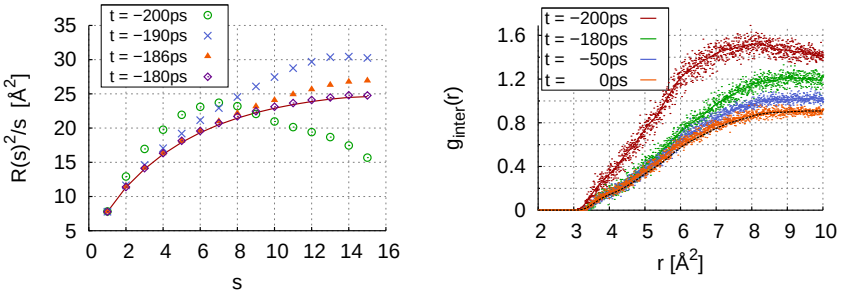

Figure 4.3: The panels above show the manner in which the chain structure develops during the deformation of the simulation box for a $N = 16$ system. The temperature is held at 550 K. Left: The internal distances equilibrate surprisingly fast. Just 20 ps after the setup the equilibrium value (solid red line) is reached. In all likelihood this is because the coil structure of the short chains in this example are predominated by the chain stiffness. Right: The inter-chain radial distribution approaches the mean value of an equilibrated melt (black dashed line) while the volume of the original all trans system is reduced.

renders PIB chains that resemble rods, see fig. 4.1. Other than the torsional angle all angles and bond lengths are set to their equilibrium values, θ_0 and l_0, which, as discussed in section 3.1, are not equal to the mean values. Hence the monomer architecture is, albeit only weakly, distorted from its relaxed structure. The coordinates of one such chain are calculated and read into LAMMPS which then clones this chain with the command `replicate x y z`. In the following the all-trans method is demonstrated on a system with 256 chains of length $N = 16$. Fig. 4.1 shows this system after applying the command `replicate 4 8 8` to one single all-trans chain to generate 256 cloned chains. It is important to note that by setting up the system with a low density this method avoids any excluded volume overlap of either inter-chain or intra-chain nature.

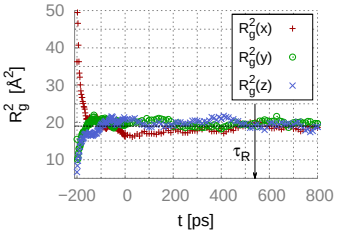

Figure 4.2: Above the time development of the radius of gyration x,y,z-components R_g^2 are shown for an all-trans setup of the $N = 16$ system. During the first 200 ps the system undergoes deformation. Starting from $t = 0$ the system equilibrates under standard conditions. The dashed line is the equilibrium value for $1/3R_g^2$ and the arrow indicates the Rouse time of the system.

Warm-up, simulation box deformation and equilibration

Given that neither the local chain structure is overly distorted nor do the beads overlap, the warm-up procedure is straightforward. There is no need to cap or toggle the interaction potentials, merely the integration step length is reduced. The preliminary equilibration is done under nvt conditions with the Nosé-Hoover thermostat. Over the course of 3000 integration steps the integration step length is increased from 0.5 fs to 2 fs. This allows the local chain structure to relax while ensuring that no unproportionally large forces give rise to skewed monomer or chain topology. In return for avoiding bead overlap the starting volume of the simulation box is set to twice the normal size. Hence after the preliminary equilibration the volume must be reduced. Still working under nvt conditions, the simulation box is deformed to a cube with the `fix deform` command. The end volume of the box is calculated from the specific volume ν, which can be estimated from experimental

values, see eq. (3.21). The deformation takes place over 200 ps for the 256×65 system ($\approx \tau_R/2$). Once the target volume is reached, this time is denoted as $t = 0$ in fig. 4.3 and fig. 4.2, the ensemble is switched to the npt regime while the thermostat stays unchanged and the system is propagated under standard conditions. To evaluate the equilibration of the melt, the time development of the components of the radius of gyration R_g^2, the intra-chain distance function $R^2(s)/s$ and the radial distribution function $g_{\text{inter}}(r)$ are monitored. The $R^2(s)/s$ distribution coincides with that of an equilibrated system just 20 ps after the system setup, as can be seen in the plot on the left of fig. 4.3. For the short chains studied here this is not a sufficient indicator for equilibrium, because the coil structure is dominated by the chain stiffness. A look at $g_{\text{inter}}(r)$, on the right hand side of fig. 4.3, reveals that the system is far from equilibrium at $t = -180$ ps. Only once the simulation box has reached its desired volume does $g_{\text{inter}}(r)$ concur with that of an equilibrated system. The time development of the R_g^2 components is pictured in fig. 4.2. It shows that at $t = 0$ the chains have recoiled considerably but the $R_g^2(x)$ component seems to be overly compressed as a result of the deformation. This example shows that it is difficult to judge when exactly the system is in equilibrium. It is advisable to let the system run for the period of a full Rouse time after completing the deformation to ensure equilibrium coil conformations. The all-trans setup is an easily executed method for short chains for which τ_R is an accessible simulation time. For longer chains, when τ_R becomes unreasonably large to simulate, this method is no longer feasible. We were successful in applying the all-trans method to chains of a degree of polymerization up to $N = 35$. Applying this method to chains of twice this length showed complications and for chain lengths of $N = 128$ and $N = 350$ we employed the fine-graining method described later in this chapter.

4.1.2 Temperature runs

The next method which is introduced is less about generating a new system but rather suggests how to speed up the decorrelation of the chain configurations of an existing system. Given an equilibrated system the chain configurations can be sampled and studied. The system should then be propagated for a period of τ_R before sampling the then decorrelated configurations. In the following an exemplary system of 128 chains of length $N = 128$ is discussed. The Rouse time of this system is $\tau_R = 160$ ns at 550 K. The longest time spans one can reasonably simulate are within 250 ns to 500 ns depending on the system size.[1] The aforementioned system would render two to three sets of independent chain configurations. The chain dynamics are considerably faster at higher temperatures. The plot in fig. 4.5 of the center of mass mean square displacement (msd) at different temperatures shows this effect.

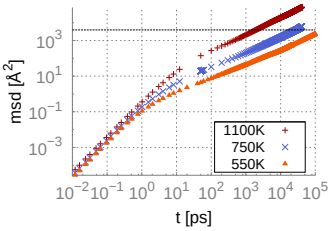

Figure 4.5: The figure shows the acceleration of the chain dynamics with increasing temperature for chain of $N = 128$ length. The mean square displacement (msd) of the center of mass is shown at different temperatures. The dashed line marks the squared end-to-end length R_{ee}^2 of the chains at 550 K.

[1] The computation time for simulating 1 ns of the example system is 4 days on one processor. We used parallel processing and were able to run systems of this size on 8 cores, propagating the system by 2 ns per day.

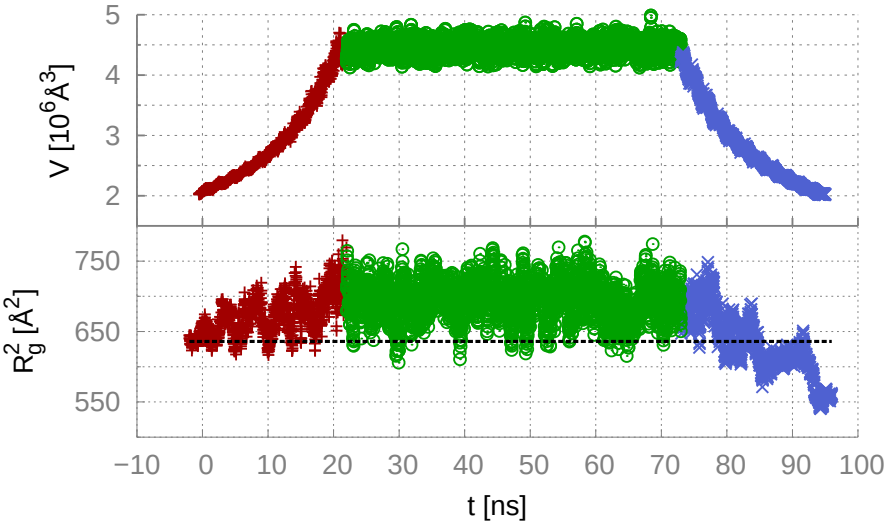

Figure 4.4: The plots above show the volume V and the squared radius of gyration R_g^2 of a system undergoing a temperature run from 550 K to 1100 K and back. After completing the temperature run R_g^2 is smaller than the equilibrium value indicated by the dashed black line. Although the cool-down is done gradually the system is over quenched and the chains are slightly compresed.

The Rouse time is two orders of magnitude smaller at 1100K than at 550K for the $N = 128$ system. It is therefore reasonable to consider warming up the system to a higher temperature, letting it run for the reduced Rouse time and then cooling it back down. Nevertheless it has to be taken under consideration that the chain structure is temperature dependent. Hence the development of the chain structure after the cool down must be monitored.

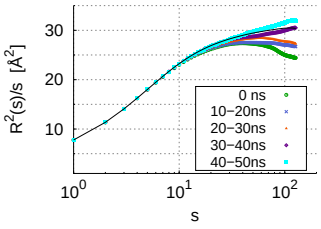

Figure 4.6: After the cool down the chain shows signs of collapse only on length scales larger than $s = 20$. The local chain structure is unaffected.

Increasing and decreasing the temperature

The temperature run is performed under npt conditions with a Nosé-Hoover thermostat. Given the temperature dependence of the melt density, the damping parameter for the barostat must be recalculated with eq. (3.18) for each temperature. The temperature is increased in steps of 50 K per ns. Each step is then followed by a 1 ns long acclimation phase at constant temperature. Once a temperature of 1100 K is reached, the system is propagated for 50 ns which is more than ten times τ_R in our example. The system is then quenched in the same fashion over a course of 22 ns. The plots in fig. 4.4 show the behavior of the system during the temperature run. After the cool-down period the coil size is smaller than the equilibrium value, as can be seen in fig. 4.7. The fact that the chain collapse occurs is only on large scales and does not effect the local monomer distribution as can be seen in fig. 4.6. This leads us to assume that the system is over quenched which gives rise to

the coils being compressed.

Equilibration

Once the system has reached 550 K it is equilibrated under standard conditions and the development is monitored. Both the intra-chain distances, see fig. 4.6, and the chain dimension, see fig. 4.7, indicate that the system is equilibrated approximately 40 ns after completing the cool down. This adds an additional $\tau_R/4$ to the simulation time. With 44 ns for warm-up and cool down, a minimum of 5 ns at 1100 K and 40 ns for the post cool-down equilibration the total run time is 89 ns= $\frac{3}{6}\tau_R$ for our example system. A slower cool down would let the chains relax more gradually and shorten the post equilibration time. It is not definit if this would shorten the total relaxation time. Though the temperature run method delivers decorrelated chain configurations in times under τ_R, for lengths upward of $N = 128$ even $\frac{3}{6}\tau_R$ poses a time length too great to achieve with standard simulation methods.

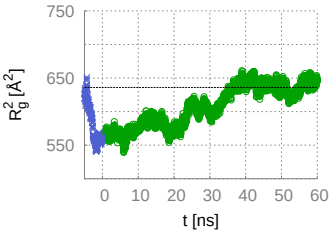

Figure 4.7: The chains collapse during the cool down and must regenerate. After 40ns, that is less then $\tau_R/3$ the chains radius of gyration equilibrates.

4.1.3 Fine-graining

So far the presented methods have proven to be unsuitable for the chain length that we aspire to simulate. To compare the simulated data with neutron scattering experiments, a chain length of at least $N = 350$ is what we aim for. Hence alternative methods of setting up a polymer melt must be explored. We were successful in employing a method termed "fine-graining" or "back mapping"[55, 56]. Fine graining is a method used to add atomistic detail to a more abstract, a coarse grained, polymer model. It combines the time efficiency of coarse-grained (CG) simulations with the more specific information one gains from simulating united atom or all atom models. A coarse grained model such as a bead spring model lacks chemical detail and it is hence much faster to equilibrate and acquire a reasonable number of independent chain configuration.

Choosing a bead spring (BS) model which is suitable for fine-graining is delicate. The overall chain structure of the CG model must be comparable with that of the PIB chain. For this we compare the intra-chain distance function of the UA system with that of a BS model adjusting for chain stiffness as necessary until a reasonably good match is found, see fig. 4.8. The UA beads are then mapped into the volume of the coarse grained beads and the local chain structure is relaxed with a warm-up routine.

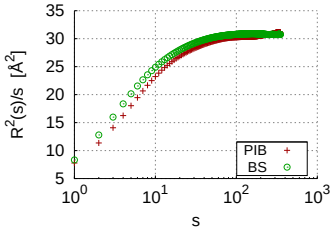

Figure 4.8: Above the intra-chain distances of an equilibrated PIB system are compared to a bead spring model which proves to be a good fit.

Preliminary considerations and the rescaling factors

Before starting the quest in search of a suitable BS model a few preliminary questions must be answered. Firstly it must be decided what the ratio λ of CG beads to UA monomers should be. It is argued that [56] it is best to choose a large λ of the order of s_p, the number of monomers per persistence length. The UA model can then be mapped onto a freely jointed chain. Though a large λ works well for single chains, in a melt

it is problematic to achieve the correct density. In our case it is of utmost importance that the coil structure as well as the melt structure are reflected correctly. For this reason the choice of a $\lambda = 1$ fine-graining, where one PIB monomer is mapped onto each CG bead, was made, see fig. 4.11. The choices for the rest of the BS parameters is discussed under the "bead spring model" section. The lengths in the CG system are measured in Lennard-Jones units (LJ) and must be rescaled to fit the PIB system. Given the importance of the melt density we define the rescaling factor γ by the volume ratio

$$\gamma = \sqrt[3]{V_{\mathrm{PIB}}/V_{\mathrm{CG}}}. \tag{4.1}$$

The volumes can be replaced by the product of specific volume ν and total system mass m

$$\gamma = \sqrt[3]{\frac{m_{\mathrm{PIB}}\nu_{\mathrm{PIB}}}{m_{\mathrm{CG}}\nu_{\mathrm{CG}}}} \tag{4.2}$$

which reduces to

$$\gamma = \sqrt[3]{((4m_{\mathrm{C}} + 8m_{\mathrm{H}})\nu_{\mathrm{PIB}})/(m_{\mathrm{LJ}}\nu_{\mathrm{CG}})} \tag{4.3}$$

where $(4m_{\mathrm{C}} + 8m_{\mathrm{H}})$ is the mass of a single PIB monomer and $m_{\mathrm{LJ}} = 1$ is the mass of a CG bead in LJ units. We assigned the specific volume of the BS system to be $\nu_{\mathrm{CG}} = 0.68\sigma^3$ and the specific volume of the PIB model can be estimated from experimental data or extrapolated from previous simulations. The rescaling factor we calculated is then $\gamma = 4.37\text{Å}/\sigma$.

The bead spring model

Finding a suitable BS system for fine-graining is intricate and involves some trial and error. We started with a fairly common BS model. In this model the excluded volume interactions are regulated by a Weeks-Chandler-Andersen (WCA) potential [57]

$$U_{\mathrm{WCA}}(r_{ij}) = \begin{cases} 4\epsilon_{ij}\left[\left(\frac{\sigma_{ij}}{r_{ij}}\right)^{12} - \left(\frac{\sigma_{ij}}{r_{ij}}\right)^{6} + c_{\mathrm{shift}}\right] & \text{if } r_{ij} \leq r_{\mathrm{cut}} \\ 0 & \text{if } r_{ij} > r_{\mathrm{cut}} \end{cases} \tag{4.4}$$

with the following parameters in Lennard Jones units (LJU)

$$\sigma_{\mathrm{WCA}} = 1 \qquad \epsilon_{\mathrm{WCA}} = 1$$
$$r_{\mathrm{cut}} = \sqrt[6]{2} \qquad c_{\mathrm{shift}} = \frac{1}{4}.$$

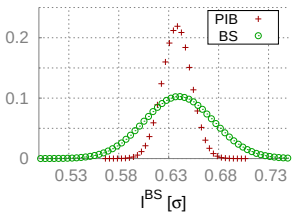

Figure 4.9: This plot shows the bond-length distribution of the BS System in comparison to the scaled carbon-carbon distances d_{CC}/γ of the UA model.

Adorned with its methyl side groups PIB is a rather bulky polymer. To emulate the girth of the PIB chain, the BS model must have a ratio of bond length l^{BS} to bead diameter σ^{BS} that is smaller than one, $l^{\mathrm{BS}}/\sigma^{\mathrm{BS}} < 1$, causing the beads to overlap. Given the $\lambda = 1$ fine-graining ratio, the distance between the quaternary carbon atoms d_{CC} in the PIB model and the bond length in the BS model l^{BS} should follow

$$d_{\mathrm{CC}} = \gamma l^{\mathrm{BS}}. \tag{4.5}$$

Following this equation the mean bond length of the BS system should be $\langle l^{\mathrm{BS}} \rangle = 0.64\sigma$. Fig. 4.9 shows that this is reached when regulating the bonds with a harmonic potential and when an equilibrium bond length of $l_0^{\mathrm{BS}} = 0.63\sigma$ is employed together with a large spring constant $K^{\mathrm{BS}} = 400$. Because of the strong volume overlap the WCA interactions between the nearest neighbors along the chain are switched off. See page 8 for a detailed discussion of "special bonds". Now that the bond lengths are adjusted, it is also necessary to find an angle potential that adds stiffness to the BS chain. The angle that is enclosed by three neighboring quaternary carbon UA beads shows a complex distribution with two maxima, see fig. 4.10. Replicating this distribution with a simple potential is impossible and, in our case, not necessary. Instead a harmonic angle potential with a spring constant $K_{\mathrm{theta}}^{\mathrm{BS}} = 4.0$ and an equilibrium value of $\theta_0^{\mathrm{BS}} = 118$ is applied. The resulting angle distribution functions can be seen in comparison with the PIB model in fig. 4.10. The BS coils that are formed by these potentials have an internal structure that is very similar to the one of the PIB chains, see fig. 4.8. Having found a BS system that is suitable for fine-graining, the next step is to determine a method to set the UA beads into the volume of the CG beads.

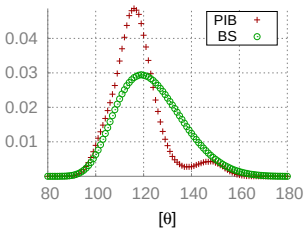

Figure 4.10: Shown here is the distribution of the angle formed by the quaternary carbon atoms of the UA model in comparison to the angle distribution of the CG system.

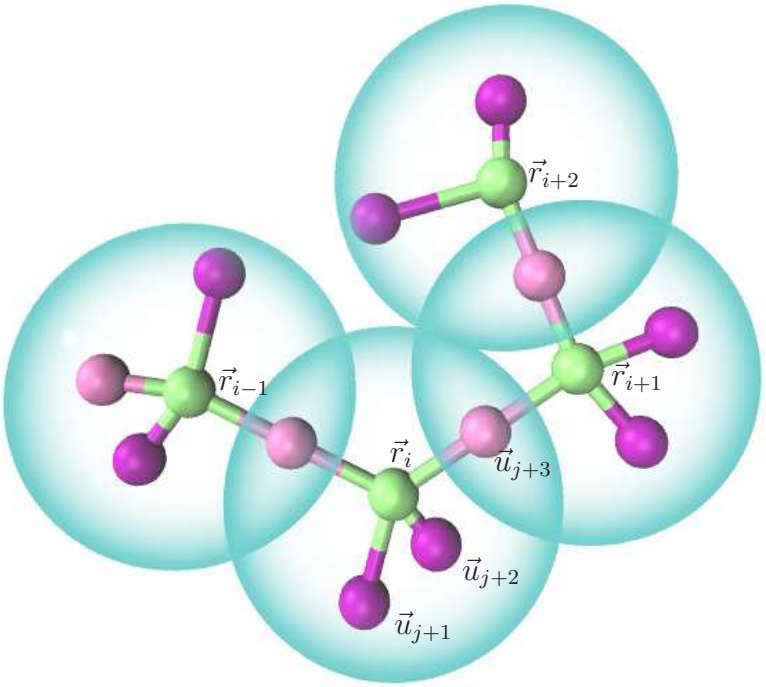

Figure 4.11: The graphic above helps to understand the fine-graining process. The large blue spheres represent the BS model into which the UA beads are set. The BS beads and the UA bonds are drawn to scale, the UA beads are drawn much smaller for reasons of legibility.

Geometry

With the chosen $\lambda = 1$ fine-graining ratio a chain with originally N_{CG} beads consists of N_{CG} PIB monomers and hence a total of $N_{\mathrm{PIB}} = (4N_{\mathrm{CG}} + 1)$ UA beads after fine-graining. To distinguish the positions of PIB and BS beads the following notation is used. The positions of the CG beads are referred to as $\vec{r}_i$ and the UA positions as $\vec{u}_j$. Fig. 4.11 shows an explanatory graphic of the fine-graining with the respective vectors. The mapping algorithm places the quaternary carbon UA bead into the center of the CG bead, that is $\vec{r}_i = \vec{u}_j$. The methylene UA groups are placed on the axes between two neighboring CG beads $\vec{u}_{i+3} = \frac{1}{2}(\vec{r}_i + \vec{r}_{(i+1)})$. This leads to the θ^{g} angle being extremely overstretched and the bonds being compressed. Trial runs show no benefit from placing the methylene bead away from the $\vec{r}_i + \vec{r}_{(i+1)}$ axis to accommodate the θ^{g} angle. In fact, it leads to unfortunate configurations where two methylene beads of neighboring chains may come too close to each other causing their excluded volume to overlap and making the warm-up process more difficult. The last step of constructing the PIB monomer is to position the methyl groups. They are placed on the open side of the $\vec{r}_{(i-1)}$–$\vec{r}_i$–$\vec{r}_{(i+1)}$ angle. The plane formed by the methyl beads and their quaternary carbon atom is perpendicular to the plane formed by the quaternary carbon atom and its adjacent methylene beads.

Warm-up and equilibration

The fine-grained chain is strongly distorted on the monomer level. To relax the compressed bonds and overstretched angles as well as the overlapping beads the fine-grained system must be carefully equilibrated. To this end a series of different integrators and restrictions are applied. Since the initial relaxation processes take place on the monomer scale, the warm-up routine introduced below works well on all fine-grained systems independent of the chain length. With exception of the excluded volume interaction of the methyl groups and the SHAKE bonds no potentials are altered during the warm-up procedure. The acting forces are regulated purely by different integration methods and reduced integration time steps. Here the warm-up routine is discussed by means of the example of a system of 256 chains with $N = 350$ monomers. The warm-up routine is composed of the following 5 blocks:

Block 1: The integrator `nve/limit` provided by LAMMPS has proven helpful to carefully propagate the system. It limits the displacements of the particles per time step, here we apply a limit of 0.01Å. The temperature is controlled by a Langevin thermostat set to $100\,K$ and the damping constant to $300\,fs$ the full command that was used is `langevin 100.0 100.0 300.0 1`. The integration time step is set to 0.2 fs, that is one tenth of the regular time step. Additionally, for the duration of the first block the carbon UA beads are fixed in space by using the `setforce 0 0 0` command to set the forces applying to the carbon atoms equal to zero. This is done so that the local chain structure can relax while conserving the melt topology. Also the size of the methyl groups is reduced by setting the LJ interaction parameter to $\sigma^{\text{methyl}} = 0.050$Å. This reduces the forces caused by overlapping methyl groups. The SHAKE algorithm is turned off for the initial equilibration, all bonds are regulated by the same harmonic potential. Under these conditions the system is integrated for a total of 150 steps. The forces acting on the methylene UA beads are so strong that they tend to "fly off" even with the limited displacement length in place. Setting all velocities to zero after 50 integration steps has proven to be an effective countermeasure. This causes the temperature to jump to zero which can be seen in fig. 4.12. At the end of block 1 the velocities are again set to zero.

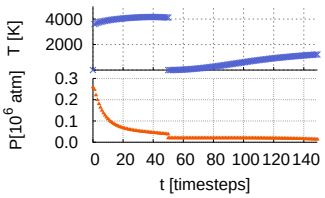

Figure 4.12: Block 1: The temperature and pressure of the first 150 integration steps of the warm-up routine are shown above. The prominent jump after 50 time-steps is due to setting the velocities to zero as a countermeasure to the strong forces acting on the methyl groups.

Block 2: Now that the gross distortion of the monomer structure has relaxed, the forces acting on the beads are considerably smaller and the carbon UA beads can be released from their constraint without fear of loosing the chain topology. The time-step is raised to 2 fs and the system is further propagated for 1000 integration steps, that is 2 ps. The development of the temperature and pressure are shown in fig. 4.13.

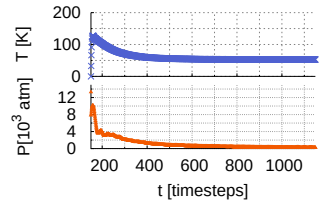

Figure 4.13: Block 2: At the beginning of the second block the carbon atoms are released from their constraint and the integration step is raised to 2 fs.

Block 3: Next the thermostat is switched to nvt Nosé/Hoover which also does the integration, so the Langevin integrator is no longer needed. The full excluded volume potential of the methyl groups is switched on at the beginning of this block. The thermostat is set to begin at 100 K and the temperature is increased over the course of 4 ps to 550 K. The parameter with which the thermostat is called are `nvt 100.0 550.0`

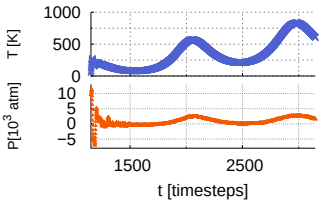

Figure 4.14: Block 3: All potentials and the integrator are switched to their regular values. The temperature is increased from 100 K to 550 K over the course of this block.

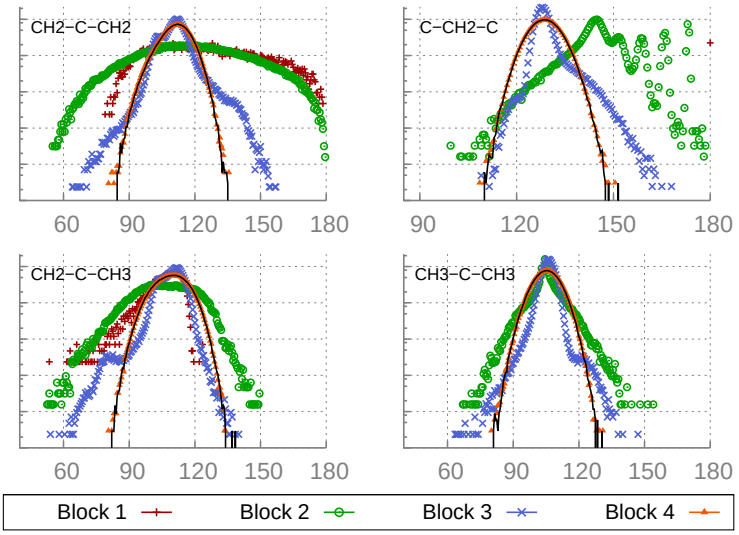

Figure 4.16: The plots show the relaxation of the monomer angles over the course of the first three blocks. The distribution functions were taken from the first frame of the respective blocks. The solid line shows the angle distribution of an equilibrated chain at 550K.

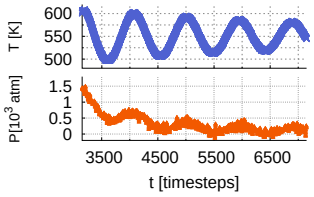

Figure 4.15: Block 4: The thermodynamic properties follow a damped oscillation during the final equilibration period under nvt conditions.

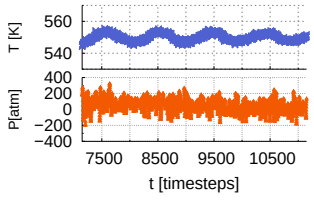

Figure 4.17: Block 5: once the system is switched to the npt ensemble the oscillations of the thermodynamic properties become much weaker. The pressure shows normal fluctuations.

`300.0`. Additionally the SHAKE algorithm is switched on to restrain the larger part of the bonds. Under these conditions the system is integrated for 2000 step. The local structure of the chain is fully relaxed at the end of this block. The development of the thermodynamic properties can be seen in fig. 4.14.

Block 4: Once the system has reached 550K, it is propagated under constant temperature with the same conditions as in block 3 for another 4000 integration steps. The thermostat parameters are `nvt 550.0 550.0 300.0`. As can be seen in fig. 4.15 the temperature and pressure oscillate during this block. The amplitude decreases and the temperature and pressure are near their equilibrium values after 8 ps.

Block 5: After a total of 7150 integration steps, that is 12.03 ps, the ensemble is switched from canonical to isothermal-isobaric in the last block. The system is run under standard conditions for an additional 8 ps. The pressure no longer oscillates and the temperature oscillations are considerably damped, see fig. 4.17. After completing the warm-up routine, the fine-grained system can be propagated as any regular system.

The local monomer structure quickly equilibrates from its distorted set-up when a careful warm-up routine such as the one described above is applied. The four different angles and their development over the course of the first three blocks is shown in fig. 4.16. At the beginning of block 4 the monomer structure is fully equilibrated. We do not include an explicit torsional stiffness to the BS model as is done for the PIB model does. Fig. 4.18 shows the development of the torsional distribution. After completing the initial three blocks of the warm-up procedure the torsional distribution is equilibrated. The long range conformation is naturally slower to equilibrate. Fig. 4.19 shows how the intrachain

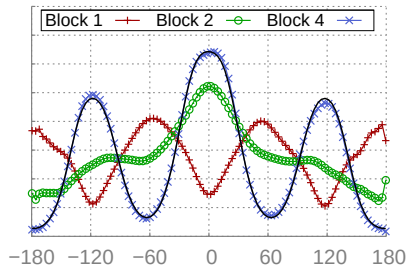

Figure 4.18: The plot shows the relaxation of the torsional distribution of the backbone. At the beginning of block 4 the torsional structure of the chains is fully equilibrated. The black line shows the equilibrated value at 550K.

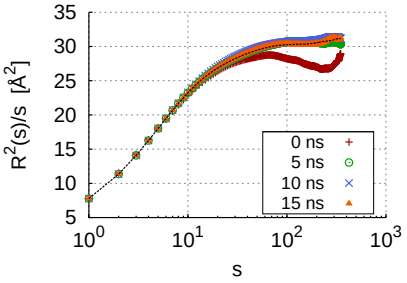

Figure 4.19: The equilibration of the long range configuration is assessed by the intrachain distance function. The solid line is the equilibrium distribution. The BS system underestimates the coils size for large s. After 5 ns the coil configuration is equilibrated.

distance function develops after fine-graining. The long range structure is equilibrated after 5 ns. The computational time saved by using fine-graining is immense. Only through fine-graining is it possible for us to simulate systems in the order of chain lengths $N = 350$. The relaxation time of $\tau_R = 1.5\,\mu$s could not be reached with conventional equilibration methods.

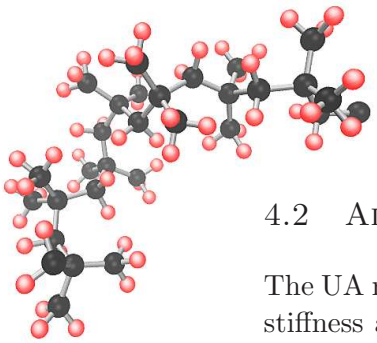

Figure 4.20: Above a PIB chain is pictured after adding the hydrogen atoms (red) to the UA model in a final step of fine-graining.

4.2 All Atom Fine-graining

The UA model of PIB provides us with information concerning the chain stiffness and coil size. The hydrogen atoms do not contribute to these quantities and hence it is justifiable to incorporate them into the UA beads. When wanting to compare the simulation results with data from neutron scattering (NS) experiments the UA model reaches its limits. The scattering data that we work with is derived from neutron scattering at the hydrogen atoms of the PIB chains. The scattering at the carbon atoms does not contribute to the scattering picture. Hence it is reasonable to add the hydrogen atoms in a final step of fine-graining, rendering an all atom (AA) description of the PIB chains. The single chain structure factor is then calculated from the newly derived hydrogen positions. The research at hand concentrates on the static prop-

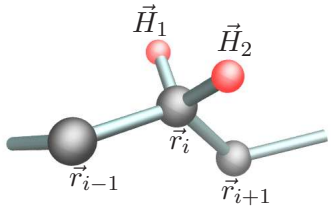

$$
\begin{aligned}
l_{\mathrm{x}} &= l\,\cos(\theta/2)\\
l_{\mathrm{y}} &= l\,\sin(\theta/2)\\
\vec{x} &= ((\vec{r}_{i-1}-\vec{r}_i)\times(\vec{r}_{i+1}-\vec{r}_i))\\
\vec{y} &= \vec{r}_i - \frac{1}{2}(\vec{r}_{i-1}+\vec{r}_{i+1})\\
\vec{H}_1 &= \vec{r}_i + \hat{e}_{\vec{x}}\,l_{\mathrm{x}} + \hat{e}_{\vec{y}}\,l_{\mathrm{y}}\\
\vec{H}_2 &= \vec{r}_i - \hat{e}_{\vec{x}}\,l_{\mathrm{x}} + \hat{e}_{\vec{y}}\,l_{\mathrm{y}}
\end{aligned}
$$

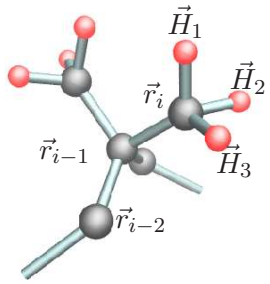

$$
\begin{aligned}
l_{\mathrm{x}} &= l\,\cos(\theta/2)\\
l_{\mathrm{y}} &= l\,\sin(\theta/2)\\
\vec{x} &= (\vec{y}\times((\vec{r}_i-\vec{r}_{i-1})\times(\vec{r}_{i-2}-\vec{r}_{i-1})))\\
\vec{y} &= \vec{r}_i - \vec{r}_{i-1}\\
\vec{H}_1 &= \vec{r}_i + \hat{e}_{\vec{x}}\,l_{\mathrm{x}} + \hat{e}_{\vec{y}}\,l_{\mathrm{y}}\\
\vec{H}_2 &= \vec{r}_i + M_{\hat{e}_{\vec{y}}}(\alpha)\,\hat{e}_{\vec{x}}\,l_{\mathrm{x}} + \hat{e}_{\vec{y}}\,l_{\mathrm{y}}\\
\vec{H}_3 &= \vec{r}_i + M_{\hat{e}_{\vec{y}}}(2\alpha)\,\hat{e}_{\vec{x}}\,l_{\mathrm{x}} + \hat{e}_{\vec{y}}\,l_{\mathrm{y}}
\end{aligned}
$$

Figure 4.21: The figures above illustrates how the hydrogen atoms of the methylene and methyl groups are added to the UA model. The angle θ is 109.5° in both cases and the bond length is $l = 1.092$Å for CH2 and $l = 1.059$Å for CH3 [58]. $M_{\hat{e}_{\vec{y}}}(\alpha)$ is the Euler rotational matrix which rotates the vector around the $\hat{e}_{\vec{y}}$ axis by an angle α which in our case is 120°.

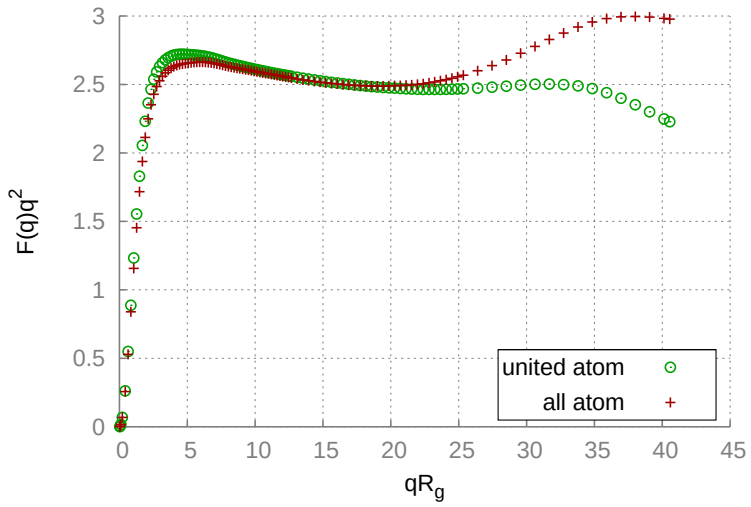

Figure 4.22: The plot shows the single chain structure factor calculated from the UA model and the AA model in comparison for chains of length $N = 350$. The data is shown in Kratky representation to emphasize the intermediate scattering lengths. R_g is the radius of gyration of the chains, q the scattering vector and $F(q)$ the intra-chain structurefactor, i.e. the formfactor.

erties of the chains. In constrast to other research [40] the AA system generated in the scope of this work are not propagated in time. Hence no force fields for the added hydrogen atoms must be defined. The hydrogen atoms are added to the PIB skeleton by defining a coordinate system relative to each methylene and methyl UA bead, see fig. 4.21. All angles and bond lengths are taken from the "CRC Handbook of Chemistry and Physics" [58]. The positions of the hydrogen atoms are fully defined by the relative angles and the bond lengths. For our purposes it is not necessary to take the thermal distribution of bonds and angles into account. Fig. 4.22 compares the formfactor calculated from the AA model with that of the UA model. In the AA model only the hydrogen atoms contribute to the structure factor. The calculation of the UA formfactor was done by applying a weighing factor to the methyl and methylene UA beads to account for the number of hydrogen atoms they represent. For small q values that hold information about the coil size the data overlap. Already at intermediate q values the difference between UA and AA chains becomes apparent. On large q scales that probe the atomistic level, the structure functions deviate strongly, as is expected. The slight, albeit significant, difference between the UA and AA structure factor on intermediate q scales justifies the elaborate step of calculating the positions of the hydrogen atoms.

The neutron scattering process, selective labeling and its influence on the structure factor are all discussed in chap 5.

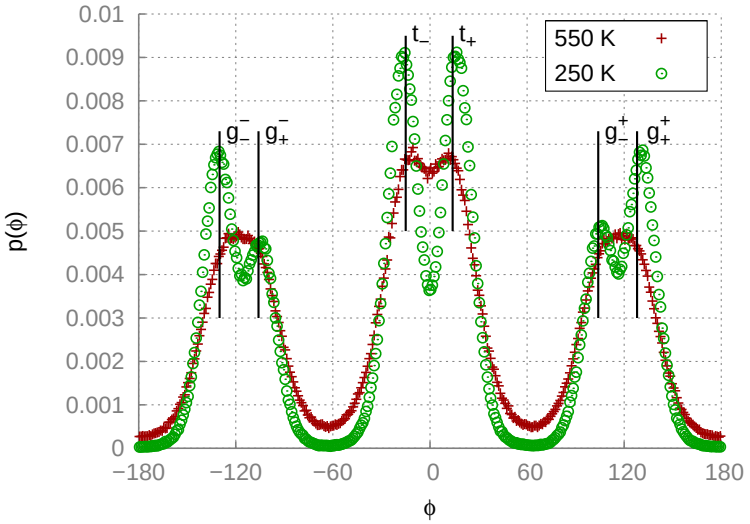

Figure 4.23: The plot shows the distribution of the dihedral backbone angles at 250 K and 550 K. The six preferred torsional states are $g_-^- = -130°$, $g_+^- = -106°$, $t_- = -15°$, $t_+ = 15°$, $g_+^- = 106°$, $g_-^- = 130°$. The lower index implies the class a bond occupies and the subscript of the gauche states indicates the position.

4.3 Rotational Isomeric State Monte Carlo Method

The rotational isomeric state (RIS) model, described in Flory's book on the "Statistical Mechanics of Chain Molecules" [3] and in a later review article [59], is a theory to calculate unperturbed conformational properties of real polymer chains. It accounts for the detailed chemical structure of the polymer, chain stiffness, and correlations of neighboring torsional angles due to short-range excluded volume effects. The RIS theory provides methods of calculating such quantities as chain stiffness and coil size solely from the torsional and angular probability distributions via matrix calculations. For other quantity such as the static chain structure factor, which is of great interest for this work, it is necessary to explicitly construct the chain. This is done by building the chain bond-by-bond, choosing the angles and dihedrals from the predetermined probability distributions. In previous [37, 39] RIS-MC studies the probability distributions were calculated from single chain energy minimization schemes. While some of these works are reproduced in chapter 7 we chose to use the probability distribution functions derived from the molecular dynamics simulations of the UA PIB model described in section 3.1.

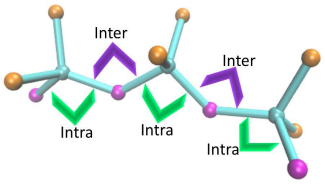

Figure 4.24: The intradiad bond pair in which both bonds occupy the t_- state is denoted as $|t_-t_-|$. The respective interdiad pair is denoted as $t_-|t_-$.

Dihedral angle distribution

The probability distribution of the skeletal dihedral bonds is a crucial factor in defining the chain stiffness and consequently the coil size. The Lennard Jones interaction between pendant methyl groups of neighboring monomers gives rise to a dihedral distribution with six preferred

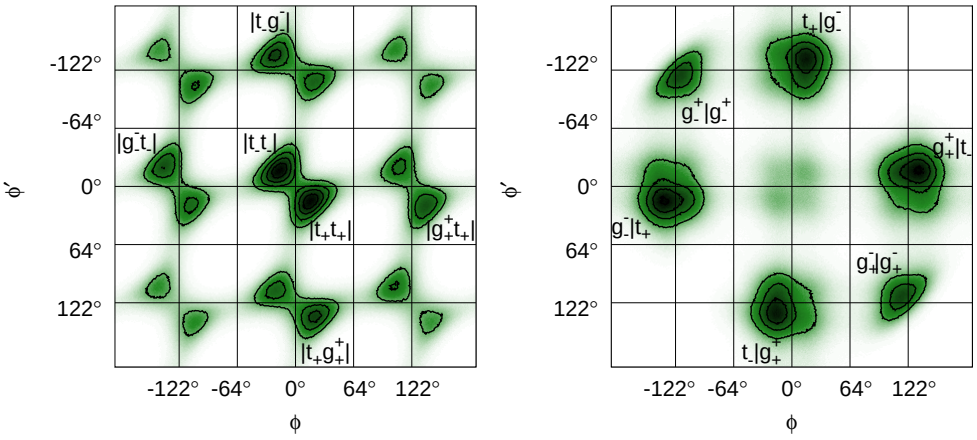

Figure 4.27: In the intradiad matrix to the left the splitting of the trans and gauche states is especially apparent. The interdiad matrix on the right provides us with essential information about the chain stiffness.

states: two trans states (t_-, t_+) and four gauche states (g_-^-, g_+^-, g_-^+, g_+^+). In the trans state the bonds are arranged to be nearly planar, see fig. 4.25 while the bonds occupying one of the gauche states are strongly twisted, see fig. 4.26. The majority of the simulations performed in the scope of this work are run at 550K. At such high temperatures the splitting of the gauche states is hardly visible. Hence, fig. 4.23 shows the torsional distribution at 250 K as well as at 550 K. The distribution at 250 K is taken from a melt which is not fully equilibrated, since relaxation times at such low temperatures are very long. We can safely assume that the local configuration is adequately, but nevertheless the torsional distribution function is used for demonstrative purposes only.

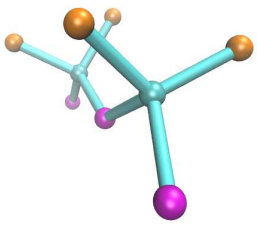

Figure 4.25: The pictured scematic PIB dimer is in trans conformation.

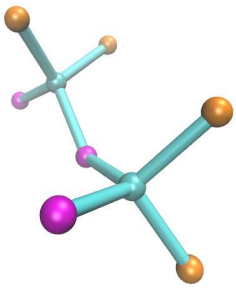

Figure 4.26: Here the dimer is in a gauche state.

For the homopolymer PIB there are two types of bond pairs: the pair centered at the methylene group, defining the intradiad matrix, and the pair flanking the quaternary C atom, which defines the interdiad matrix, see fig. 4.24. The bonds of each pair are correlated. Their joint probability distribution maps are shown in fig. 4.27. The chain ends influence the torsional distribution, so we droped the contributions of six end monomers and calculated the probability maps from the remaining 232 bonds of a $N = 128$ system at 550 K. The intradiad probability distribution is qualitatively similar to that of previous RIS studies [37, 39]. The intradiad pairs prefer the $|tg|$ states which make up for 63.6% of the population followed by the $|tt|$ states which 19% of the pairs occupy. In general states with mixed classes, such as $|t_-g_+^-|$, are very unlikely. The interdiad map on the other hand is significantly different from the most recent RIS model of PIB presented by Vacatello et al. [39]. In our model it is more likely that the bonds of an interdiad pair occupy states of different classes. The Vacatello model on the other hand prefers interdiad pair that share a class. The pairs of $t_\alpha|g_\alpha$ constellation occupy 79% of the states in Vacatellos model as opposed to the 34.6% in our model. The most heavily populated stated in our model are of the $t_\alpha|g^\beta$ type, accounting for 41% of the interdiad pairs.

Numerical Methods

The random number generator we implemented for the MC simulations is the "Shift Register Generator" R250/512 [60] which provides us with good uniformly distributed random numbers $0 \leq \mathrm{RN} < 1$. These numbers can be converted into random variables, in our case bond angles (θ) and dihedrals (ϕ) distributed according to the probability densities mentioned above by following the procedure detailed in "Numerical Recipes" [61, pp. 277]. For an arbirary bond angle θ this involves the following steps:

Firstly the probability density function $p(\theta)$ is numerically integrated over $0 \leq \pi \leq \theta$,

$$P(\theta) = \int_0^\theta \mathrm{d}\theta p(\theta) \text{ with } P(\pi) = 1. \tag{4.6}$$

This integral gives the cumulative probability $P(\theta)$ that the random variable takes a value smaller than θ. The second step consists in drawing a uniform random number RN and in determining the θ value which satisfies $P(\theta) = \mathrm{RN}$. The procedure is adapted for the dihedral distribution maps as follows. The integration

$$Q(\phi, \phi\prime) = \int_{-\pi}^{\theta} \mathrm{d}\phi q(\phi, \phi'), \tag{4.7}$$

where $q(\phi, \phi')$ is the conditional probability that if a bond is in the dihedral state ϕ' the following bond will be in the state ϕ, is performed over every ϕ'. Then, as above the dihedral ϕ is chosen which satisfies $Q(\phi, \phi') = \mathrm{RN}$. The probability distribution functions we utilized are of high resolution. The bond angle probability distribution has a 0.1° resolution and the dihedral maps have a 1° resolution.

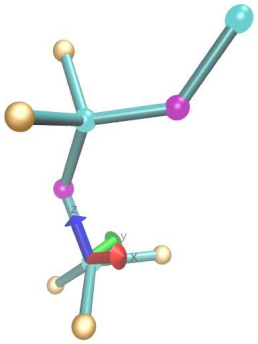

Figure 4.28: Above the beginning of a PIB chain constructed with the RIS-MC method is shown.

Building the chain

The RIS-MC simulations require that we choose the angles and dihedrals from the predetermined distributions as we build the PIB chain bond-by-bond. The bond length is assumed to be fixed at $l = 1.54$Å for all bonds. The first bond of every chain is fixed by placing the first quaternary carbon atom at the origin and the following methylene group at $(0, 0, l)$, see fig. 4.28. The second quaternary carbon atom is placed in the x, z-plane, the angle the first two bonds form is chosen according to the $p(\theta^{\mathrm{g}})$ distribution, see fig. 3.7. The position of the second methylene group is determind by choosing the backbone angle according to the angle distribution, $p(\theta^{\mathrm{a}})$, and the dihedral angle from the simple torsional angle distribution $p(\phi)$. It is the first dihedral to be specified and hence it cannot be chosen from the dihedral distribution map. Starting with positioning the fifth UA bead the dihedral angles are pulled from their respective probability maps, $q(\phi, \phi')$. The methyl group positions are calculated with respect to the $p(\theta^{b,c,d,e,f})$ angles afixing the pendant groups to the quarternary carbon atom. The entire chain is built this way, picking the dihedral bonds alternately from the inter diad and

the intradiad probability matrices. The backbone angles as well as the angles defining the position of the methyl groups are picked from the simulation data at 550 K.

The RIS-MC method does not account for excluded volume interaction and the chain tends to overlap on long length scales. The RIS-MC method is a one shot MC simulation, no energy minimization is performed, every generated chain is taken into account. Every chain is independent of the next. This allows to produce a vast amount of independent coil structures in a very small amount of time. Flory's theory is that the excluded volume in a bulk chain is shielded, so the RIS-MC chains should properly represent the bulk chains. Note that this MC procedure is a "simple sampling" MC simulation: A generated chain conformation corresponds directly to an equilibrium (RIS) configuration. Since the chain conformation generated in the next run is completely independent of the previous one, the statistical error of averages calculated over all conformations decreases as $1/(\text{total number of conformations})^{1/2}$. RIS-MC simulations are thus very fast relative to standard melt simulations.

4.3.1 Selfconsistency check

Flory offers a method to calculate the intrachain distance function for a hindered rotational chain (HRC) inside the framework of the RIS theory. We check if the data from the RIS-MC chains coincide with the RIS theory. The dihedrals of a HRC are not correlated and hence we use the $p(\phi)$ distribution in fig. 4.23 to generate the chains for comparison with the predictions [3]. The backbone angles are all set to $\theta = 120°$. The expected internal distance distribution is [62]

$$\begin{aligned} R^2(s)/s = & \left[\langle\hat{b}^2\rangle - \langle\hat{b}\rangle^2\right] l^2 \\ & + \frac{\langle\hat{b}\rangle^2 l^2}{\lambda_2 - \lambda_1}\left\{(\alpha+\lambda_2)\frac{1+\lambda_1}{1-\lambda_1} - (\alpha+\lambda_1)\frac{1+\lambda_2}{1-\lambda_2}\right\} \\ & - \frac{1}{s}\frac{\langle\hat{b}\rangle^2 2l^2}{\lambda_2 - \lambda_1}\left\{(\alpha+\lambda_2)\frac{\lambda_1 - \lambda_1^{s+1}}{(1-\lambda_1)^2} - (\alpha+\lambda_1)\frac{\lambda_2 - \lambda_2^{s+1}}{(1-\lambda_2)^2}\right\} \end{aligned} \quad (4.8)$$

with $\alpha = \cos(\theta)$ and the variance of the bond vectors $\left[\langle\hat{b}^2\rangle - \langle\hat{b}\rangle^2\right] = 0$ because the bond length is fixed to l. In eq. (4.8) the following substitution is used

$$\lambda_{1,2} = -\frac{1}{2}\alpha(1-\eta) \pm \frac{1}{2}\sqrt{\alpha^2(1-\eta)^2 + 4\eta}\,. \quad (4.9)$$

The average over the torsional angle distribution is

$$\langle\cos\phi\rangle = \eta = \frac{\int_0^{2\pi} cos\phi\, p(\phi)\mathrm{d}\phi}{\int_0^{2\phi} p(\phi)\mathrm{d}\phi} \quad (4.10)$$

From the excelent agreement between simulation and theory, see fig. 4.29, we can be assured that the RIS-MC algorithm is implemented correctly.

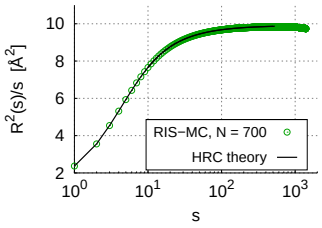

Figure 4.29: The plot show the intra chain distances of RIS-MC chains constructed with our algorithm. The backbone angle is fixed to 120° and the dihedral angles are chosen from the 550 K distribution in fig. 4.23. The solid line shows the predicted behavoir for a HRC model, eq. (4.8).

5 | Neutron Scattering Methods

Over the last decades neutron scattering has contributed largely to our understanding of the structure and dynamics of soft matter systems. This is because thermal neutrons have a de Broglie wavelength that matches interatomic distances in ordered or disordered condensed matter structures. With small angle neutron scattering (SANS) the structure can be probed on a micrometer to nanometer length scale which matches well with typical size distributions in soft matter systems ranging from polymer aggregates, micelles, to nanopores. Furthermore, thermal neutrons have an energy which is on the same order of magnitude as quasiparticle excitations. With quasielastic neutron scattering (QENS) and neutron spin echo (NSE) techniques dynamical processes become accessible, such as local vibrations, librations, and diffusion that span time scales from pico- to milliseconds.

Scattering of thermal neutrons by matter is dominated by the interaction of neutrons with the nuclei of the matter. For each isotope the neutron-nuclei scattering potential is different. Hence the scattering amplitude or scattering length is specific to the isotope, not to the atomic number, as it is in x-ray scattering. Because the neutron is a spin 1/2 particle, the scattering can be coherent or incoherent. This is a unique property in neutron scattering. With the coherent cross section the pair correlation and structural information can be gained, whereas with the incoherent cross section the self-correlation is explored. For hydrogen and its isotope deuterium the distinction between coherent and incoherent scattering lengths and thus cross sections is of particular significance. The hydrogen nuclei has a spin 1/2, so the scattering is mostly incoherent. The deuterium nuclei has a total spin +1 and it scatters mostly coherently. The total nuclear spin for the carbon isotope ^{12}C is zero, so it scatters only coherently. Isotope labeling makes use of the large difference in the scattering lengths between hydrogen and deuterium. Most polymers and organic materials are composed of carbon and hydrogen. Selectively exchanging some hydrogen nuclei in the sample for deuterium offers the possibility of making structures visible that would otherwise be difficult to detect. The chemical properties, however, are almost unaffected by isotope labeling. Measuring the single chain conformation of polymers in bulk is an example of a quantity that can only be measured by neutron scattering. If the χ parameter, which measures the miscibility of hydrogen and deuterated polymer chains, is zero, they are fully mixed and entangled and probe the conformation in its unperturbed state[63, 64]. For the polymers studied in this thesis,

we assume the χ parameter to be close to zero.

This chapter gives a short introduction to scattering physics and explains the SANS experiment performed by our collaborators[1]. The effects that chain length, stiffness and cross section have on the scattering picture are discussed on the example of chains generated with the rotational isomeric state (RIS) method. Taking these effects into account the form factor of the chains is extracted from the scattering intensity and the size of the chains is determined by comparing them to polyisobutylene (PIB) chains simulated with molecular dynamics (MD).

5.1 Neutron Scattering - Theory

The key quantity in scattering experiments is the momentum transfer $\vec{q}$, that is the difference between the incident vector $\vec{k}_\mathrm{i}$ and the scattered wave vector $\vec{k}_\mathrm{s}$

$$\vec{q} = \vec{k}_\mathrm{s} - \vec{k}_\mathrm{i}\,. \tag{5.1}$$

In the following only quasi elastic scattering experiments are discussed where there is no energy transfer between the neutron beam and the sample. Hence the wave length λ of the neutrons is unchanged by the scattering event and we can write

$$\left|\vec{k}_\mathrm{s}\right| \approx \left|\vec{k}_\mathrm{i}\right| = \frac{2\pi}{\lambda} \tag{5.2}$$

which leads to

$$|\vec{q}| = \frac{4\pi}{\lambda}\sin\vartheta \tag{5.3}$$

with 2ϑ the scattering angle. Because of this relationship $\vec{q}$ is also referred to as the scattering vector.

The scattering amplitude $A(q)$ depends on the scattering length b_i of the particle located at $\vec{r}_i$

$$A(q) = \sum_{i=1}^{\mathcal{N}_\mathrm{m}} b_i \, \exp[\mathrm{i}\vec{q}\cdot\vec{r}_i] \tag{5.4}$$

where $\mathcal{N}_\mathrm{m}$ is the total number of particles that contribute to the scattering. Experimentally the amplitude is of course not accessible. Instead the Intensity $I(q) \propto |A(q)|^2$ is measured which implies that the phase is lost during the scattering event. Thus with scattering only pair correlations can be determined but not absolute positions of atoms or nuclei in space. The scattering intensity depends on the number of scatterers. To compare results from different samples the structure factor $F(q)$ is introduced with I_m the scattering intensity of a single scatterer

$$F(q) = \frac{I(q)}{I_\mathrm{m}\mathcal{N}_\mathrm{m}} = \frac{1}{\mathcal{N}_\mathrm{m}}\sum_{i,j}^{\mathcal{N}_\mathrm{m}} \exp[i\vec{q}\cdot(\vec{r}_i - \vec{r}_j)]. \tag{5.5}$$

[1] Prof. Mark Dadmun and Dr. Caleb Deyer, University of Tennessee, Knoxville

Since the scattering centers are small compared to the volume, we change to a continuum representation with $\sum_{i,j}^{\mathcal{N}_\mathrm{m}} \rightarrow \int_V$ so that

$$F(q) = \frac{1}{\langle\rho\rangle} \int_V \exp[i\vec{q}\cdot\vec{r}](\langle\rho(r)\rho(0)\rangle - \langle\rho\rangle^2)\mathrm{d}^3\vec{r} \tag{5.6}$$

in which $\vec{r} = \vec{r}_i - \vec{r}_j$ and $\rho(r)$ is the local density of scatterers. From this equation it becomes apparent that scattering only takes place at density fluctuations.

To emphasize the relationship between the scattering picture and the structure of the sample eq. (5.6) can be written as

$$F(q) = \int_V \exp[i\vec{q}\cdot\vec{r}](g(\vec{r}) - \langle\rho\rangle)\mathrm{d}^3\vec{r}, \tag{5.7}$$

where $g(r)$ is the pair distribution function which is defined as [51, p. 391]

$$g(\vec{r}) = \frac{\langle\rho(\vec{r})\rho(0)\rangle}{\langle\rho\rangle}. \tag{5.8}$$

Eq. (5.7) shows the well known identity that the structure factor is the Fourier-transform of the pair distribution function.

In the following we describe a small angle scattering experiment on PIB chains. The samples investigated consist of a blend of deuterated and protonated PIB chains. As already mentioned, the scattering intensity is due to composition fluctuations. It is possible to directly probe the single chain scattering function, i.e. the form factor of a single chain by contrast variation of the blended PIB chains [64]. In the case of Gaussian chains the pair distribution function is

$$g(\vec{r}) = \left(\frac{3}{2\pi\langle\vec{r}^2\rangle}\right)^{3/2} \exp\left(-\frac{3\vec{r}^2}{2\langle\vec{r}^2\rangle}\right). \tag{5.9}$$

When plugging eq. (5.9) into eq. (5.7) the integral can be evaluated and the result is the Debye function $D(x)$ [51, p. 33]:

$$F(q) = \frac{2\mathcal{N}_\mathrm{m}}{(qR_\mathrm{g})^4}\left[\mathrm{e}^{-(qR_\mathrm{g})^2} - 1 + (qR_\mathrm{g})^2\right] = \mathcal{N}_m D(Q = qR_\mathrm{g}). \tag{5.10}$$

The Debye function can be approximated in the limits of very small and very large Q as

$$D(Q) = \begin{cases} 1 - Q^2/3 & \text{for} \quad Q \ll 1 \\ 2/Q^2 & \text{for} \quad Q \gg 1\,. \end{cases} \tag{5.11}$$

These approximations together with the Debye function are shown in fig. 5.1. The small Q range is also known as the Guinier regime. Scattering in the Guinier regime is often used to determine the radius of gyration and degree of polymerization of the chains. The larger Q-regime holds information about the internal coil structure. A $F(q) \propto 1/q^2$ behavior is expected for ideal chains, and hence scattering data of polymer systems is often shown in the Kratky representation, plotting $Q^2F(q)$ vs. Q. The so-called Kratky plateau for $Q > 2\pi$ is often interpreted as proof of ideality in real chains. Though it has been noted, as is discussed in the following sections, that "[...] Kratky plots have to be interpreted with care" [63, p.252].

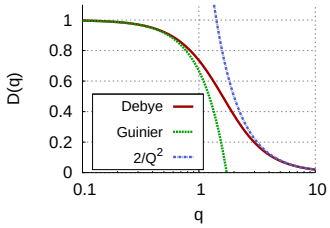

Figure 5.1: The Debye function (solid line) and its approximations, see eq. (5.11).

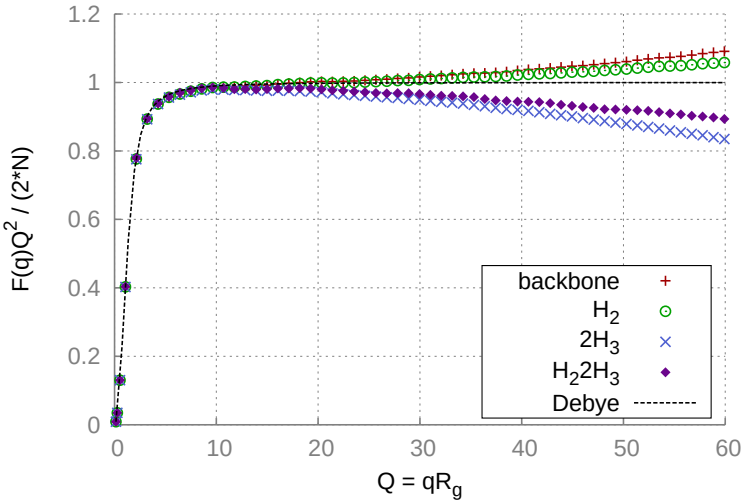

Figure 5.2: The figure above shows the influence of the chain cross-section on the structure factor. The structure factor has been calculated with respect to four different scattering centers. The data denoted as "backbone" is the structure factor solely regarding the carbon atoms along the backbone of the chain. With "H_2" we denote the structure factor gained by regarding only the hydrogen atoms belonging to the methylene group. The data denoted "$2H_3$" take only the hydrogen atoms belonging to the methyl groups into consideration, and the data denoted "$H_2 2H_3$" take into account all hydrogen atoms of the chain. The solid line shows the Debye function eq. (5.10). All form factors are calculated from the rotational isomeric state (RIS) model with potentials derived from the molecular dynamics simulation of PIB at 550 K chains of length $N = 11200$.

5.1.1 The real chain

The section above discusses the structure factor of an ideal chain, neglecting effects of chain stiffness and cross-section that influence the scattering picture. In the following we quantitatively introduce properties of real chains that lead to deviations from the Debye curve. To distinguish between the different effects we resort to chains generated by the RIS-MC method detailed in section 4.3. These chains are unperturbed by excluded volume effects and are Gaussian for large N. Also the RIS-MC chains are generated much faster than the MD chains and hence it is possible to access an array of very long chain lengths.

The influence of labeling

Theoretical considerations of polymers often start from the idealization that polymers consist of point-like monomers that, strung together, form string-like coils. This is justified by assuming the cross-section, i.e. the girth, of the chain to be much smaller than the total chain length. Contrary to this beliefe, neutron scattering experiments on selectively labeled chains have shown that the cross-section strongly influences the form factor. That this effect is not limited to high q-values has been

demonstrated in the work of Rawiso et al. [65], who studied differently labeled polystyrene. They show that the form factor of backbone labeled polystyrene deviates from that with labeled phenyl rings for q-values as low as $q = 0.03$Å. The influence of selective labeling on the form factor is also discussed in "Polymers and Neutron scattering" [63] in which the authors warn that the effects of chain stiffness and cross-section may superimpose, leading to a plateau in the Kratky regime that can be falsely interpreted as a sign of chain ideality. We study this effect by comparing the form factor of modeled PIB chains with different scattering centers, see fig. 5.2. For small Q-values the form factors for all four different types of labeling collapse onto the Debye curve, signifying ideal chain behavior. For larger Q-values the form factors deviate from the Kratky plateau. The backbone and methylene labeled chains show an upward deviation from the Kratky plateau, typical of a rod-like objects. The form factor of the methyl groups and the fully labeled chain ($2H_3$ and $H_2 2H_3$) show a downward deviation from the Kratky plateau. This type of labeling makes the cross-section of the chain visible. Scattering from the methyl groups is comparable to scattering from a tube-like object rather than from point-like monomers. The effect of the cross-section of the chain overpowers the stiffness effect.

Rawiso et al. introduced a method to derive the form factor of a point-like chain from the scattering signal of a chain with a notable girth using the following formula [65, eq.(37)]

$$F'(q) = F(q) \exp\left[-q^2 R_c^2/2\right] \tag{5.12}$$

with $F(q)$ the original and $F'(q)$ the reduced form factor. The radius R_c is the radius of gyration of the chain with respect to the backbone axis. When considering the scattering signal of the hydrogen atoms of PIB, R_c can be approximated as a hollow cylinder with diameter equal to the distance between the methyl and methylene hydrogens. This estimation gives us the value of $R_c = 1.25$ Å. In fig. 5.3 this method is successfully applied to the RIS-MC chains to reduce the form factor of the fully labeled chain to that of the backbone labeled chain. This opens the possibility of treating chains as infinitely thin, even if their form factor was originally measured by labeling atoms that are located at a finite distance from the chains axis.

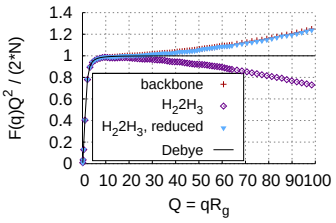

Figure 5.3: With the method explained in [65] the effect of the chain cross-section can be factored out.

Finite length effects

The persistence length l_p of the RIS-MC chains of the current work (c.w.) is 4.13 Å, see chapter 7. It is expected that the chain stiffness affects the form factor on q-scales that probe distances comparable to l_p. Fig. 5.4 shows the form factor of RIS-MC generated chains ranging in lengths from $N = 350$ up to $N = 89600$. Only the backbone atoms are considered in this plot to avoid interfering effects caused by the chain cross-section. All chains, independent of their length, deviate from the Debye curve at approximately $q = 0.09\,\text{Å}^{-1}$, which translates into a spacial distance of 70 Å. The radius of gyration of the two shorter chains shown in fig. 5.4 is smaller than 70 Å. The form factor of these chains

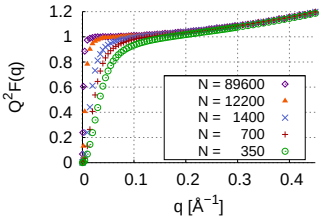

Figure 5.4: The form factor of the backbone deviates from the Kratky plateau of chains of varying length, demonstrating the influence of chain length on the form factor. The from factor is calculated from the backbone carbon atoms.

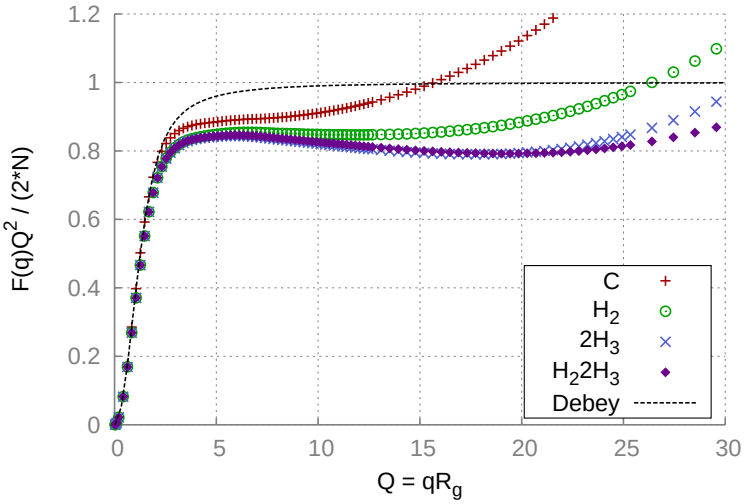

Figure 5.5: The plot shows the form factor of the $N = 350$ chains simulated with MD methods at 550 K. The notation of the different labeling is the same as in fig. 5.2.

shows no plateau in the Kratky regime. The Kratky plateau is only visible for much longer chains with $R_g > 70$ Å. The chain stiffness affects larger length scales than we assumed. The longest chains simulated by molecular dynamics are of length $N = 350$, hence the structure factor is strongly influenced by the chain stiffness. Additionally to the cross-section and the chain stiffness, the MD simulations of PIB also takes into account the excluded volume interaction. A quantity that is intrinsically neglected by the RIS-MC chains. In fig. 5.5 the form factor of the MD chains of length $N = 350$ is shown with different types of labeling. The excluded volume interaction leads to a depression in the Kratky region. All effects combined lead to an alleged Kratky plateau for the fully labeled chain, though this false plateau is at $Q^2F(q)/(2N) \approx 0.8$ rather than 1. The absence of a real Kratky region for PIB chains of length $N = 350$ makes the analysis of the residual excluded volume effects more difficult.

5.2 Neutron Scattering - Experiment

5.2.1 The samples

The SANS measurements that are discussed in the following were preformed by our collaborators, the group of Prof. Mark Dadmun from the University of Tennessee in Knoxville. Two different chain lengths were studied which will will denote as “long” and “short” in the following. Protonated and deuterated polyisobutylene (h-PIB and d-PIB) samples were synthesized by Prof. Robson Storey (University of Southern Mississippi). The d-PIB samples are fully deuterated, meaning that all hydrogen atoms of the methyl and methylene groups are replaced by deuterium. The samples were dissolved in tetrahydrofuran (THF) and

	N_n	N_w	PDI
d-PIB, short	273	284	1.04
h-PIB, short	328	341	1.04
d-PIB, long	622	659	1.06
h-PIB, long	672	785	1.02

Table 5.1: The characteristics of the PIB samples measured by the MALL/SEC method directly after synthesis.

analyzed by multiangle laser light scattering (MALL) and size exclusion chromatography (SEC). The results for the number-average degree of polymerization N_n, the weight average N_w and the polydispersity index $PDI = N_w/N_n$ are listed in table 5.1.

Supposedly an error occurred during the analysis of the deuterated chains so that over half a year after the first analysis the samples were reevaluated using the 100% mass recovery method and the results presented in table 5.2 were obtained. As to this date confusion around the

	N_n	N_w	PDI
d-PIB, short	349	363	1.04
d-PIB, long	822	838	1.02

Table 5.2: Reevaluation of the deuterated chain leads to a higher degree of polymerization.

two different sets of data is not resolved and since the samples have been destroyed, performing a third analysis is impossible.

From the four chain types, a totalof six samples were prepared. Four samples contain the purely protonated and deuterated samples while the remaining two contain a blend of the hydrogenated and deuterated PIB of one length. The structural information is gained from the blended sample since the protonated sample only scatters incoherently, while the deuterated sample scatters mainly coherently. The measurements of the pure samples are needed to subtract the incoherent scattering from the blended sample. The volume fraction ϕ of d-PIB in the blended samples was determined by the transmission intensity and is

$$\phi(\text{d-PIB,S}) = .503 \quad \phi(\text{d-PIB,L}) = .510\,. \tag{5.13}$$

The mixing properties of two polymers can be quantified by the Flory-Huggins parameter χ. A positive χ value leads to immiscibility, which can happen between deuterated and protonated polymer chains. F. Bates et al. [66] discuss the phenomena of demixing in deuterated and protonated polymers by the example of polybutadiene. In previous scattering experiments on d-PIB and h-PIB [17] the χ parameter was found to be zero, allowing for the chains to mix. For the samples at hand the density was measured and the relationship $\rho_D = 1.1\rho_H$ veryfied.This implies that the density of the deuterated monomers is only increased by the addidtional neutrons, but the monomer volume stays unchanged. Since immiscibility is often due to different monomer volumes, this anal-

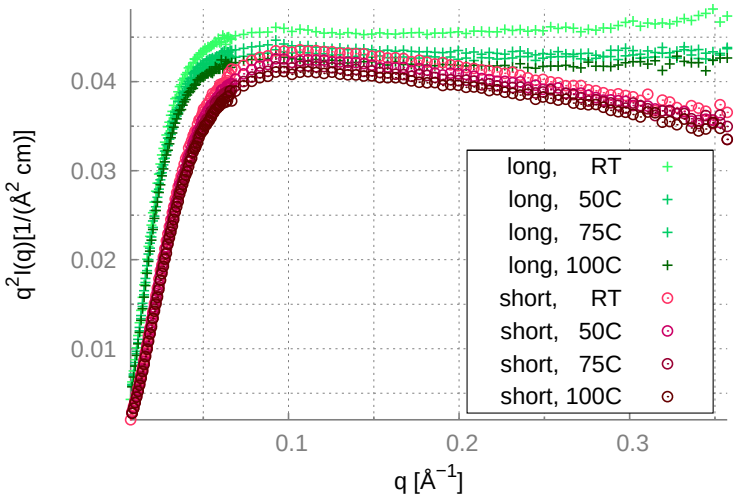

Figure 5.6: Intensity versus q after data reduction. The temperature dependence stems from the density variance.

ysis gives further weight to the assumption that $\chi = 0$ for d-PIB and h-PIB.

5.2.2 Neutron Scattering and Data Reduction

The scattering experiment took place at the 30m SANS machine **NG-7** at the National Institute of Standards and Technology (NIST) facility in Gaithersburg, Maryland. The scattering intensity was measured by a position sensitive helium detector. By varying the sample-to-detector distance it was possible to sample a q-range of $0.00829\,\text{Å}^{-1}$ to $0.3572\,\text{Å}^{-1}$. The samples were placed in a heatable sample holder. The PIB samples themselves were contained in 1 mm thick cells. Both sets of samples were measured at four different temperatures: at room temperature ($\approx 25°\text{C}$), 50°C, 75°C, and 100°C. The purpose of heating the sample was that the chain stiffness as quantified by C_∞ decreases with increasing temperature, rendering a more flexible polymer at higher temperatures. However, the effect is very weak and the difference of C_∞ at 100°C and 25°C is less then 1% according to Fetters et al. [31] .

The scattering from the samples containing pure d-PIB and pure h-PIB as well as the blended samples were measured at each temperature. The scattering from the empty cell was also measured. Additionally the background events were measured by blocking the beam. The results from these measurements are then used to extract the coherent scattering of the blend by applying the following method of data reduction

$$I(q) = (I_{\text{blend}} - I_{\text{cell}}) - \phi(I_{\text{d}} - I_{\text{cell}}) - (1-\phi)(I_{\text{h}} - I_{\text{cell}}) - I_{\text{background}}\,. \quad (5.14)$$

$I(q)$ is the intensity of the coherent scattering of the blended sample. The raw data after reduction is shown in fig. 5.6. The temperature dependency is clearly visible.

5.2.3 Data Analysis

After preforming the data reduction described above the SANS measurements provide the coherent scattering intensity $I(q)$ of the blended sample. To extract the form factor from the scattering intensity we apply the random phase approximation (RPA) described in [63, p. 404].

$$I(q) = k_\mathrm{n}\Big[\frac{1}{v_\mathrm{H}\phi_\mathrm{H}F_\mathrm{H}(q)} + \frac{1}{v_\mathrm{D}\phi_\mathrm{D}F_\mathrm{D}(q)} - 2\chi/v_0\Big]^{-1}. \tag{5.15}$$

The factor $k_\mathrm{n} = N_\mathrm{a}\left(a_\mathrm{H}/v_\mathrm{H} - a_\mathrm{D}/v_\mathrm{D}\right)^2$ results from the incompressibility constraint of the melt. This is well justified because the composition fluctuations of the hydrogen and deuterium species are much larger than the density fluctuations of the melt. The parameters and functions appearing in eq. (5.15) have the following significance:

- N_a is the Avogadro Number: $N_\mathrm{a} = 6.0221415 \cdot 10^{23}\ \mathrm{mol}^{-1}$.
- a_H and a_D are the coherent scattering lengths of the protonated and deuterated monomers. Their values are $a_\mathrm{H} = -3.3408\,\mathrm{fm}$ and $a_\mathrm{D} = 79.952\,\mathrm{fm}$.
- v_H and v_D are the volumes of the protonated and deuterated monomers. We take them as

  $$v_\mathrm{H} = \frac{m_\mathrm{H}}{\rho_\mathrm{H}} \quad \text{and} \quad v_\mathrm{D} = \frac{m_\mathrm{D}}{\rho_\mathrm{D}}, \tag{5.16}$$

  where $\rho_\mathrm{H} = 0.928505\,\mathrm{g/cm}^3$ and $\rho_\mathrm{D} = 1.021355\,\mathrm{g/cm}^3$ are the monomer densities of h-PIB and d-PIB. For ρ_H we use a parametrization of eq. (3.21) and applied the empiric relationship of $\rho_\mathrm{D} = 1.1\rho_\mathrm{H}$ which was verified for the samples at hand.
- The volume v_0 is an arbitrary reference volume. Following Beaucage et al. [67] we take $v_0 = \sqrt{v_\mathrm{H}v_\mathrm{D}} = 61.62845\mathrm{cm}^3/\mathrm{mol}$.
- χ is the Flory-Huggins (segment-segment) interaction parameter, as discussed above. Though it is known that for isotopic mixtures in general, we may not assume χ to vanish [66], [63, p. 137], density analysis of the samples at hand suggest χ to be zero in the case of d-PIB and h-PIB.

For the following analysis we rewrite eq. (5.15) as

$$I(q) = K(T)\Big[\frac{\phi_\mathrm{D}}{v_\mathrm{H}/v_0}\frac{1}{F_\mathrm{H}(q)} + \frac{\phi_\mathrm{H}}{v_\mathrm{D}/v_0}\frac{1}{F_\mathrm{D}(q)}\Big]^{-1}. \tag{5.17}$$

with the temperature dependent factor $K(T)$:

$$K(T) = \left[\frac{a_\mathrm{H}}{v_\mathrm{H}/v_0} - \frac{a_\mathrm{D}}{v_\mathrm{D}/v_0}\right]^2 \frac{\phi_\mathrm{H}\phi_\mathrm{D}}{v_0} = 0.176134\,\rho_\mathrm{H}(T). \tag{5.18}$$

The density is temperature dependent as is shown in eq. (3.21). We assume that the h-PIB and d-PIB chains of one sample have the approximate same chain length and polydispersity, which is justified when

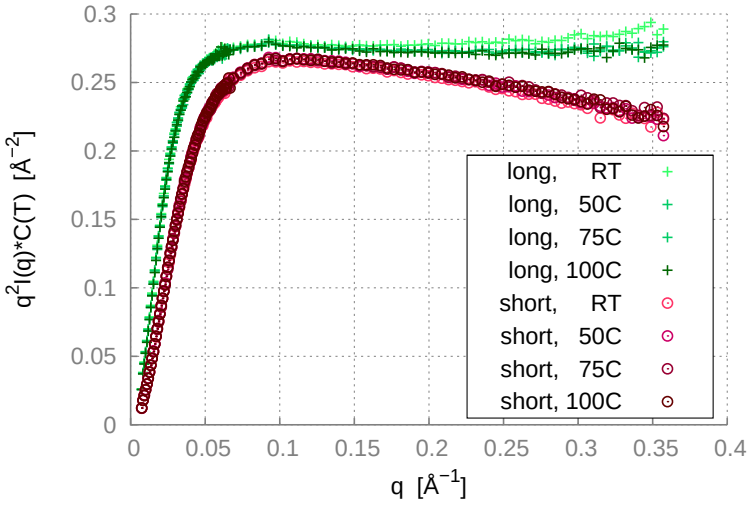

Figure 5.7: The Kratky plot for the structure factor of the chains at different temperatures collapse onto one master curve. This shows that only the density, but not the coil structure is influenced by the temperature in the studied regime.

assuming the first sample analysis to be true. Further we assume the form factors of h-PIB and d-PIB to be the same

$$F_{\mathrm{H}}(q) = F_{\mathrm{D}}(q) = F(q). \tag{5.19}$$

For eq. (5.17) this implies

$$\frac{1}{K(T)} I(q) = C(T) I(q) = F(q) \tag{5.20}$$

because

$$\frac{\phi_{\mathrm{D}}}{v_{\mathrm{H}}/v_0} + \frac{\phi_{\mathrm{H}}}{v_{\mathrm{D}}/v_0} = 1.00058. \tag{5.21}$$

When converting the intensity to the form factor with the temperature dependent proportionality factor $C(T)$ the curves for the different temperatures collapse with exception of the sample measured at room temperature, see fig. 5.7. The exact temperature the sample had during this measurement is not known. We approximated it to be 25°C, but since it is not coherent with the other data, this particular set of data will be dropped from further analysis.

Determining the coil size by a Guinier fit

Traditionally the chain size is extrapolated by fitting the Guinier approximation to the very small q values. This analysis method is applied to the data from every temperature separately. The chosen fit range is between $q^2 = 8 \cdot 10^{-5}\text{Å}^2$ and $q^2 = 15 \cdot 10^{-5}\text{Å}^2$. The mean values for the degree of polymerization and the coil size are summarized in the table of fig. 5.8 together with the fit itself. $R_{\mathrm{g,z}}$ is the z-average radius of gyration. Surprisingly the degree of polymerization that is assigned to

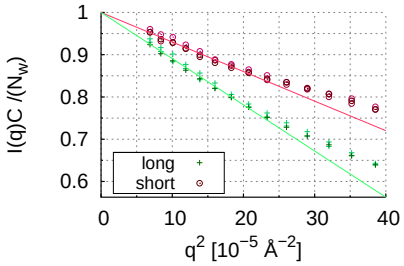

	N_w	$R_{g,z}$[Å]	C_∞
short	271	45.8	9.7
long	585	57.3	7.1

Figure 5.8: The values of chain length and radius of gyration gained from fitting the Guinier approximation at small q are listed in the table. The actual fit is shown in the plot on the left, where the data of all temperatures collapse onto one curve.

the chains from this fit is lower than what is expected from the previous analysis (cf. tables 5.1 and 5.2). The chain stiffness can be extracted from the fitted values by applying

$$C_\infty = 6R_g^2 \frac{1}{b_0^2 2N} \tag{5.22}$$

were $b_0 = 1.53\,\text{Å}$ is the bond length [2]. The values of the C_∞ are listed in the table of fig. 5.8. These values indicate that the PIB chains are stiffer than what is suggested in the literature [31], where $C_\infty \approx 6.5$.

To test the viability of the values extracted from the Guinier fit, we display them in a normalized Kratky plot together with the MD simulation data. The data is expected to collapse onto a master curve, but as can be seen in fig. 5.9 this is not the case. Though the longer chain coincide quite well with the simulation data, the form factor of the shorter chains lies above the Debye curve. This leads us to believe that in the q-region in which the Guinier fit is performed the real chain effect (cross-section, finite length, excluded volume) cause a deviation from the Debye curve.

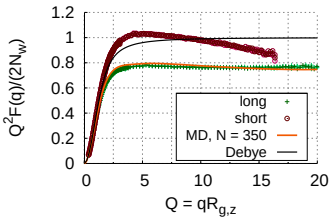

Figure 5.9: The Kratky plots are normalized with the values of the Guinier fit in fig. 5.8 and compared to the chains simulated with molecular dynamics.

Determining the coil size by camparison to the simulation data

Since the SANS measurements performed do not span lower scattering angles we resort to manually fitting the SANS data to the MD data of the longest simulated chains, that is $N = 350$. We do this by choosing the radius of gyration and the degree of polymerization so that the form factor of the SANS data and that of the MD data coincide. Fig. 5.10 shows the fitted SANS data together with the MD data. The results of the fit are summarized in the table of fig. 5.11.

The values returned by this method are in good agreement with the chain characterization done by SEC/MALLS (cf. table 5.1). In the normalized Kratky plot the data of the two real PIB samples and the simulated chains collapse onto one curve for small q-values, see fig. 5.11. Only by means of the united atom (UA) simulations of PIB and the consequential adding of the hydrogens could the SANS data be successfully interpreted. The traditional fit of the Guinier approximation at

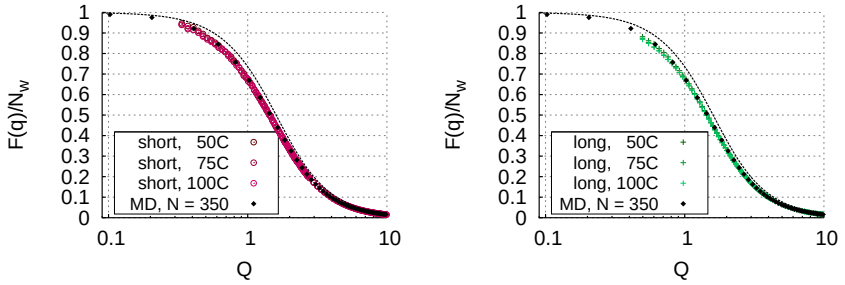

Figure 5.10: Manually fitting the SANS data to the $N = 350$ MD simulated chains in the low q-regime. The results are summarized in table 5.11

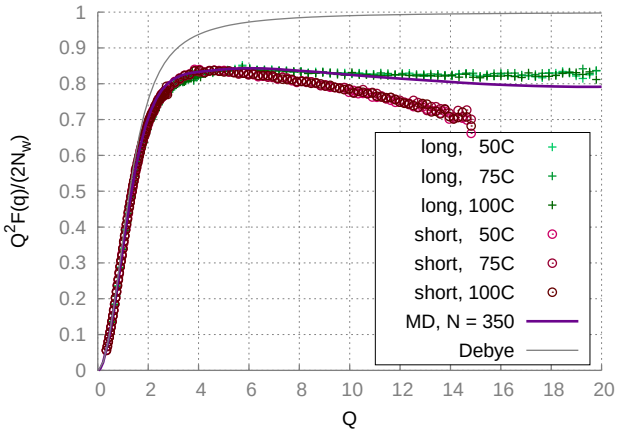

	N_w	$R_{\mathrm{g,z}}$[Å]
short	275	41.5
long	653	62

Figure 5.11: Comparison of the NS and MD data in Kratky representatio. The values above a taken from the manual fit of the SANS data to the structure factor of the simulated chains at 550 K.

low q-values failed, because the cross-section of the chain influences the form factor even in the smallest q regime that was measured. In the following discussion the values of table fig. 5.11 will be used.

6 | Deviations from ideality in chain structure

The Flory ideality hypothesis states that flexible polymer chains in a melt assume the shape of three-dimensional random walks leading to so-called Gaussian coils. The basis of this hypothesis is that any local conformational information, i.e. bond angles or torsional angles, decays exponentially along the chain backbone and thus has no influence on the long range conformation. Additionally it is argued that the excluded volume shielding of neighbor chains cancels out any swelling effects. Neutron scattering (NS) experiments dating back 30 years confirm the postulated Gaussian coil shape of polymers [17]. This leads to a pillar of polymer theory: Any flexible polymer, independent of its chemical structure, can, after appropriate rescaling, be described as a three-dimensional random walk. This assumption was utilized in describing the chain characteristics of our model PIB chains in chapter 3.

Figure 6.1: In 1974 Paul Flory won the Nobel prize for his work in the field of chemistry. His intuitive approach to polymer science and disarmingly simple argumentation have formed today's understanding of the amorphous structure of polymers and macromolecules.

Advances in simulation techniques and computing power have opened the door to the possibility of studying very long chains. This allowed for a closer look at the chain structure of polymer melts and revealed deviations from ideality. This deviation is very slight and thus great care must be taken to distinguish it from noise. So far the deviation from the Gaussian coil structure was only studied for coarse-grained models [68]. The scope of this thesis is to explore if these deviations are also measurable in atomistically realistic simulations and modern day NS experiments.

In the following chapter we will discuss if the corrections to ideality are detectable in our PIB model. Firstly we explore the deviations in real space by studying the orientational correlation function of the bonds along a chain. Then we switch to reciprocal space to compare our simulation data with NS experiments.

The ideal chain

The ideal chain, much like the ideal gas, is a strongly simplified model. Both neglect certain aspects of the physical reality but are nevertheless capable of making very good predictions in a specific domain [69]. The ideal chain is asymptotically long and has neither excluded volume nor orientational correlation beyond the first bond. As discussed in detail in [1] the segments of an ideal chain follow a Gaussian distribution. Let $\vec{r}_s$

be the spatial distance between the segments n and m with $s = |n - m|$ the number of segments separating them. The probability distribution function is then

$$\Phi(\vec{r}_s, s) = \left(\frac{3}{2\pi}\frac{1}{sa^2}\right)^{3/2} \exp\left(-\frac{3}{2}\frac{\vec{r}_s^{\,2}}{sa^2}\right) \tag{6.1}$$

with a the segment length. While the first moment of the distribution is zero, $\langle \vec{r}_s \rangle = 0$, the second moment holds information about the coil size of the segment

$$\langle \vec{r}_s^{\,2} \rangle = R^2(s) = a^2 s, \tag{6.2}$$

where $R^2(s)$ is the mean-square internal distance function. Its second derivative is the bond-bond correlation function, $P_1(s)$ [8, eq. (3)]. In the case of the ideal chain there are no correlations and it is, as mentioned before, zero. This can easily be shown by plugging eq. (6.2) into

$$P_1(s) = \frac{\langle \vec{b}_n \cdot \vec{b}_m \rangle}{\langle \vec{b}^2 \rangle} = \frac{1}{2b^2}\frac{\mathrm{d}^2}{\mathrm{d}s^2} R^2(s) \tag{6.3}$$

and one gathers for the ideal chain $\frac{\mathrm{d}^2}{\mathrm{d}s^2} a^2 s = 0$. If the chain has an angle or torsional stiffness as is the case for any real polymer, and assuming that information is passed solely along the backbone, the segment length can be rescaled so that eq. (6.2) and eq. (6.3) hold. In section 3.2 we applied the freely rotating chain (FRC) model to the simulated PIB chains with very convincing results. The equations for the internal distance distribution, see eq. (3.17), and the bond-bond orientational correlation function, see eq. (3.15), of the FRC converge towards eq. (6.2) and eq. (6.3) respectively for $s \gg 1$.

Excluded volume screening

In [3] Flory argues that a real polymer chain in a melt of equal chains can be described by the ideal chain model. The reasoning is that any chemical detail can be neglected after appropriate rescaling and the excluded volume of the chain can be ignored due to the screening effect of the melt. The concept of the excluded volume screening can best be understood when starting from a chain in a good solvent [1, p. 24]. The coil configuration then arises from the balance of two effects: the interaction energy of the excluded volume and the elastic energy stemming from the connectivity of the chain. While the interaction term leads to a swelling of the chain, the entropic term leads to a shrinking. This gives rise to a coil structure that can be compared to a self avoiding walk with $R \propto N^{3/5}$.

In a dense melt each chain is surrounded by monomers of the same interaction potential. Let us consider the conformation of a test chain submerged in a melt. The energy of the system is comprised of the energy of the host system, U_{melt}, the elastic energy U_{entro} and the excluded volume energy U_{excl} of the test chain and finally a term that attributes the interaction between test chain and host melt U_{inter}. The sum over these contributions is then the total energy of the melt U_{total}

$$U_{\mathrm{total}} = U_{\mathrm{melt}} + U_{\mathrm{entro}} + U_{\mathrm{excl}} + U_{\mathrm{inter}}\,. \tag{6.4}$$

De Gennes visualizes this mean field approach with the correlation hole effect [70, pp.54]. At the basis of the correlation hole argumentation is the assumption that a dense polymer melt is nearly incompressible and density fluctuations are negligible. The concept of the correlation hole is quite simply that, given the incompressability constraint, two segments cannot occupy the same space at once, since this would lead to a higher density at that point. Following de Gennes' argumentation we start with the excluded volume interaction of the test chain. While the probability to find a segment that belongs to the test chain is high at the center of mass of said chain, it decreases rapidly for distances of the order R_g, as depicted in fig. 6.2. The pair correlation function $p_{\text{intra}}(r)$ measures the probability of finding a segment which belongs to the test chain itself at a distance r from its center of mass. From $p_{\text{intra}}(r)$ we can derive the interaction potential $U_{\text{excl}}(r) = -k_B T \ln p_{\text{intra}}(r)$, which is the excluded volume energy of the test chain that leads to a swelling of the chain. The next energy contribution we explore is the interaction energy between the melt and the test chain. Given the restraint of constant density, the probability of finding a segment that does not belong to the test chain is $p_{\text{inter}}(r) = 1 - p_{\text{intra}}$ and therefore $U_{\text{inter}}(r) = -k_B T \ln(1 - p_{\text{intra}}(r))$. The interaction term shrinks the polymer and we may picture the chains of the melt pushing the test chain back, hindering the swelling. The sum over the interaction energy and the excluded volume energy is then

$$U_{\text{excl}}(r) + U_{\text{inter}}(r) = -k_B T \Big(\ln p_{\text{intra}}(r) + \ln\big(1 - p_{\text{intra}}(r)\big) \Big). \quad (6.5)$$

The self-density $\rho^*(r)$ of the test chain is very small because it pervades a large volume $\propto R^3$ so that $\rho^*(r) \simeq N/R^3 \ll \rho$ where ρ is the total density of the melt. Substituting $p_{\text{intra}}(r) = \rho^*(r)/\rho$ into eq. (6.5) we write

$$U_{\text{excl}}(r) + U_{\text{inter}}(r) = -k_B T \Big(\ln\big(\rho^*(r)/\rho\big) + \ln\big(1 - \rho^*(r)/\rho\big) \Big). \quad (6.6)$$

With $\rho^*(r)/\rho < 1$ we can use the approximation $\ln x \simeq (x-1)$ and write

$$\begin{aligned} U_{\text{excl}}(r) + U_{\text{inter}}(r) &\simeq -k_B T \Big(\big(\rho^*(r)/\rho - 1\big) + \big(1 - \rho^*(r)/\rho - 1\big) \Big) \\ &= k_B T \end{aligned} \quad (6.7)$$

resulting in an energy term independent of r. The total force $F(r) = \frac{\mathrm{d}}{\mathrm{d}r} U(r)$ acting on the test chain is zero because the excluded volume is effectively screened by the melt. Hence the coil structure is formed purely by the entropic energy term which leads to an ideal chain configuration with $R \propto N^{1/2}$.

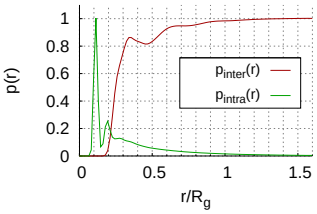

Figure 6.2: Above the correlation hole is visualized by the inter and intra chain radial distribution functions. The distribution functions are calculated from the quaternary carbon atoms of a $N = 128$ melt at 500 K.

6.1 Corrections in real space

In recent years the possibility of large scale computer simulations has allowed for a more detailed investigation into the structure of polymer coils under bulk conditions. Numerical studies [5–9] and analytic calculations [5, 71, 72] have reconsidered the excluded volume screening argumentation. The assumption that conformational information

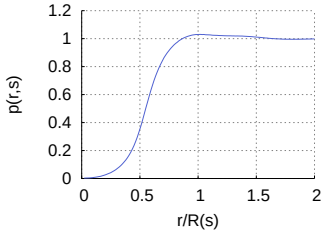

Figure 6.3: Pair distribution function of subchains of length $s = 9$ belonging to $N = 128$ chain at 550 K. Contrary to the ideality hypothesis the distribution function is not constant in r but shows that the subchains repel each other at length scales $1 < r/R(s)$. For distances $r > 0.7R(s)$ the probability is larger than unity due to the connectivity of the chain.

is solely passed along the length of the chain and hence must always decay rapidly is incorrect. Given the incompressibility restraint, conformational information is also passed directly through the melt and the two segments n and m are more strongly correlated than purely by the information passed along the bonds.

Let us revisit the correlation hole effect but this time we consider the interaction between subsegments of the test chain. Let $p(r, s)$ be the pair distribution function of subsegments of length $1 \ll s \ll N$. The mean field approach discussed above suggests that the excluded volume is fully screened by the melt and the interaction between subsegments is zero. Hence under these assumpions, the probability distribution will be constant with $p(r, s) = p(\infty, s)$ and the interaction potential between the segments $U(r, s) = -k_{\mathrm{B}}T \ln\big(p(r, s)/p(\infty, s)\big)$ would be zero. But in contrast to this we find that the segments are subject to a repulsive potential, albeit a weak one, on length scales $r < R(s)$ (see fig. 6.3). The residual excluded volume interaction between subsegments can be estimated as

$$\frac{1}{k_{\mathrm{B}}T}U(r, s) = -\ln\big(p(r, s)/p(\infty, s)\big) \tag{6.8}$$

$$\simeq 1 - \frac{p(r, s)}{p(\infty, s)} \tag{6.9}$$

$$\simeq 1 - \frac{\rho - \rho^*(r, s)}{\rho} = \frac{\rho^*(r, s)}{\rho} \tag{6.10}$$

with $\rho^*(r, s)$ the self density of the subchain and ρ the total density of the melt. For large s the interaction potential can be estimated by

$$U(r, s) \propto \rho^*(r, s) \simeq \frac{s}{R^3(s)} \simeq \frac{s}{s^{3/2}} = \frac{1}{\sqrt{s}}. \tag{6.11}$$

The considerations above hold for chain segments s which are not connected, i.e. separate chains, as well. The perturbation to ideality is thus weak but long ranged and decreases rapidly for large s. It leads to a swelling of the chain on intermediate length scales while the intrachain distance distribution converges towards that of an ideal chain for large s. The perturbation is independent of the total chain length N, it is scale free. In principle, the same argumentation can also be repeated for $s = N$, leading to a repulsive interaction between two chains of the melt of order $1/\sqrt{N}$ and thus correcting the classical argument by de Gennes given above. However, for large N these corrections are very weak, albeit visible for coarse-grained models [68].

The swelling on the intermediate length scales, caused by the residual excluded volume interaction, affects the intrachain distance function $R(s)$

$$\frac{R^2(2s) - 2R^2(s)}{2R^2(s)} \propto U(s) \propto \frac{1}{\sqrt{s}}. \tag{6.12}$$

This has been shown for highly flexible coarse grained models [6], but in the case of the PIB chains the intrachain distance function is heavily dominated by the chain stiffness, see fig. 3.12. The simulated chains are too short in comparison to their persistence length to successfully

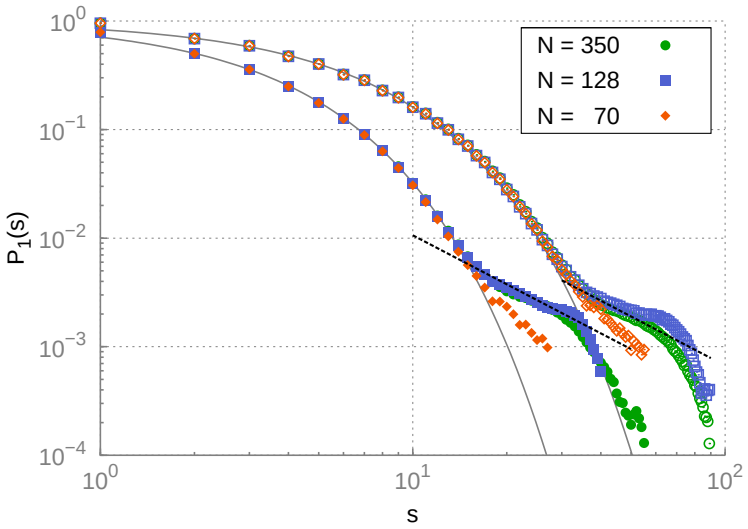

Figure 6.4: The figure shows the bond-bond correlation function for different chain lengths of PIB. The solid symbols represent the correlation between the monomers and the empty symbols represent the correlation between the backbone bonds. The dashed black lines indicate the $s^{-3/2}$ behavior expected for non-ideal chains. For chains of length $N = 70$ the influence of the residual excluded volume is almost lost in noise while it is clearly visible for longer chains with $N = 128$ and $N = 350$.

show the influence of the residual excluded volume effects on the chain structure in this manner. In lieu thereof we focus on the bond-bond correlation $P_1(s)$, see eq. (6.3), which is the second derivative of the intrachain distance function.

Perturbation calculation

As stated above the residual excluded volume interaction is very weak and can therefore be treated as a perturbation to the ideal chain. As detailed in [5, 6, 8, 73, 74] in first order perturbation any quantity $\mathscr{A}$ that is under the influence of a small perturbation $\mathscr{U}$ can be written as

$$\langle \mathscr{A} \rangle \simeq \langle \mathscr{A} \rangle_0 + \langle \mathscr{U} \rangle_0 \langle \mathscr{A} \rangle_0 - \langle \mathscr{U} \mathscr{A} \rangle_0 \tag{6.13}$$

where the averages denoted by $\langle \cdots \rangle_0$ are preformed over the unperturbed system. In our case we would like to study the bond-bond correlation function so $\mathscr{A} = P(s)$ and under the assumption that the information decays exponentially we write

$$\langle \mathscr{A} \rangle_0 \propto \exp\left(-s/s_\mathrm{p}\right) \tag{6.14}$$

with s_p the number of segments per persistance length. As discussed in [8] the perturbation caused by the correlation hole effect leads to a power law dependency with

$$\langle \mathscr{U} \mathscr{A} \rangle_0 \propto -\left(\frac{s_\mathrm{p}}{s}\right)^{3/2}. \tag{6.15}$$

In the following we neglect the mixed term $\langle \mathscr{U} \rangle_0 \langle \mathscr{A} \rangle_0$. The bond-bond correlation function decays exponentially for small s and follows the power law behavior $s^{-3/2}$ for intermediate s, as can be seen in fig. 6.4. The correlation function $P_1(s)$ has already decayed to $\approx 10^{-3}$ before the influence of the perturbation becomes visible. A considerable amount of statistics were needed to distinguish the signal from the noise.

The bond-bond correlation function is a good quantity to show the effect of the non-ideality on the chain structure, but it is not experimentally accessible. Hence we must turn to the single chain structure factor, i.e. the form factor, to compare our simulation results with experimental data.

6.2 Corrections in reciprocal space

The verification of the non-ideality in real chains by means of the form factor is challenging. Coarse grained polymer model such as the bead spring (BSM) or bond fluctuation model (BFM) have no angular or torsional stiffness and no crossection. Were it not for the residual excluded volume interaction the pair distribution function would be Gaussian and the form factor would follow the Debye curve, see 5. Instead the deviations from ideality lead to a depression in the Kratky regime of the form factor. The difference between the ideal Debye curve and the actual form factor of the chains due to corrections to chain ideality can be quantified as [8]

$$\delta\left(\frac{1}{F(q)}\right) \equiv \frac{1}{F(q)} - \frac{1}{F^0(q)} = \frac{1}{32}\frac{|q|^3}{\rho} \tag{6.16}$$

with ρ the particle number density and $F^0(q)$ the unperturbed form factor. In the case of the above mentioned coarse grained chains $F^0(q)$ is the Debye function. The q^3 dependency of the relationship in eq. (6.16) is exhaustively studied for coarse grained model polymer chains. The form factor of BFM chains of varying length is shown in fig. 6.5 and fig. 6.6. The left hand side shows the data in Kratky representation, the right hand side quantifies the deviation of the form factor from the Debye curve with

$$m(q) = \frac{\rho R_\mathrm{g}^3}{N}\,\delta\left(\frac{N}{F(q)}\right). \tag{6.17}$$

The $m(q) \propto q^3$ dependency of the BFM chains for $q > 2\pi$ validates the hypothesis of residual excluded volume effects giving rise to changes in coil conformation. Though the scaling is universal, at close inspection a chain length dependency is visible which shifts the $m(q)$ curve of shorter chains to slightly lower values. Using the construct of the Kuhn segment length we calculate which BFM chain length is comparable to our PIB chains. As discussed in section 3.2 the length of a Kuhn-segment for the simulated PIB chains is $a_\mathrm{K} = 11.25$Å. With a monomer length of $a_\mathrm{b} = 2.788$Å, this leads to a PIB chain with $N = 350$ monomers consisting of $N_\mathrm{K} = 86.7$ Kuhn-segments. The BFM chains have a characteristic ration of $C_\infty = 1.52$ [8]. A BFM chain which compares to the PIB

chain would then be of length $N^{\mathrm{BFM}} = 1 + C_\infty N_\mathrm{K} = 134$. The BFM chain closest in length would thus be the $N^{\mathrm{BFM}} = 128$ chain. The form factor of this BFM chain is compared to the to our PIB chains of length $N = 350$ in fig. 6.7 and fig. 6.8.

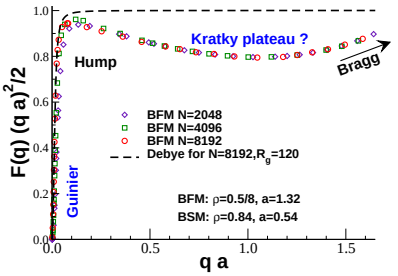

Figure 6.5: The form factor of BFM chains of varying length in Kratky representation. The depression in the Kratky plateau due to the non-ideality of the chain structure is apparent. Data taken from [7, Fig. 3]

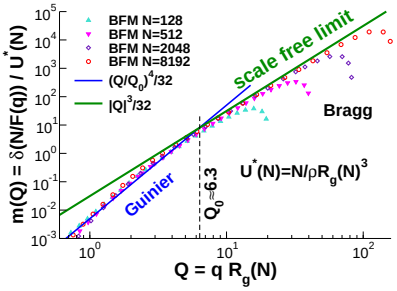

Figure 6.6: The function $m(Q)$, eq. (6.17), highlights the q^3 dependency of the deviations from ideality. Data taken from [7, Fig. 4].

Analyzing the form factor of the PIB chains poses to be more delicate. As discussed in section 5.1.1 for the $N = 350$ chains the stiffness has a strong influence on the intermediate length scales. The Debye function is not a good approximation for the PIB chains studied here within as becomes apparent in fig. 5.4. Here we suggest to replace $F^0(q)$ in eq. (6.17) with the form factor of a PIB chain of comparable length generated by the RIS-MC method, since the RIS-MC chains are generate by neglecting the excluded volume, but accounting for the correct torsional distribution. The plot in fig. 6.7 shows the form factor of the simulated PIB chains in comparison with the Debye function and the form factor of the RIS-MC chains. Naturally the curve of the RIS-MC chain is closer in form to the simulated chains than the Debye function. In fig. 6.8 the $m(q)$ vs. Q plot is shown where $m(q)$ is calculated in two different ways. When setting $F^0(q) = F^{\text{RIS-MC}}(q)$ the $m(q)$ function is closer to the BFM data. This suggests that the perturbation calculation might achieve better results for realistic polymers if the form factor generated by RIS-MC methods $F^{\text{RIS-MC}}(q)$ is used as the reference unperturbed chain as opposed to the Debye function.

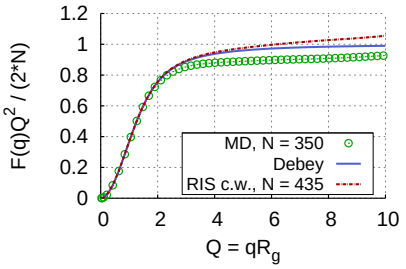

Figure 6.7: The form factor of the backbone of the UA model of PIB chain $N = 350$, and the form factor of the chains produced by the RIS-MC method in comparison to the Debye curve. The RIS-MC chains account for the early onset of chain stiffness which the Debye curve does not do.

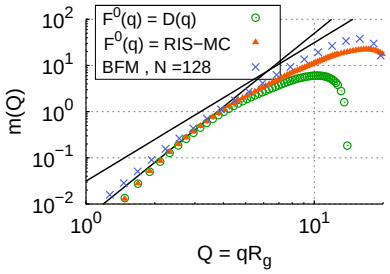

Figure 6.8: The gray lines show the q^4 and q^3 power laws. The function $m(q)$ is calculated for the $N = 350$ chain in two different ways. Once the form factor is compared to the Debye function and once to the form factor of RIS-MC chains of comparable length. The data from the BFM chain with $N^{\mathrm{BFM}} = 128$ is also shown for reference.

The method to extract information on the non-ideality effect from the form factor which is so successful for coarse grained chains falls short when applied to atomistically realistic chains. Though we were successful in showing that the PIB chains are influenced by the residual excluded volume in real space, see fig. 6.4, we are unable to do the same in reciprocal space, see fig. 6.7.

The goal is to show the effects of non-ideality in real polymer chains through neutron scattering experiments. In previous work [17, 39] the scattering results of polymer melts have been compared directly with chains generated by RIS-MC calculations. The good agreement of RIS-MC chains and scattering picture led to reinforce Flory's ideality hypothesis, see fig. 7.4. In the following we will compare the MD simulations, the RIS-MC calculation and the NS data directly to each other, showing that the MD simulations deliver the best results. Fig. 6.9 shows the form factor of PIB chains of length $N = 276$ and $N = 615$ gained by SANS measurements, see fig. 5.11. The neutron scattering was performed on a blend of fully deuterated and fully protonated chains. Hence the hydrogen atoms were added to the simulated UA chains in a final step of fine graining. For information on the hydrogen fine-graining see 4.2. The form factor was then calculated with respect to the explicit hydrogen atoms. Additionally to the chains simulated with MD methods, we also generated chains with the RIS-MC method, using both the torsional maps of the MD simulations (RISK) or the torsional maps suggested by Vacatello and Yoon (RIS-VY)[39]. From the comparison in fig. 6.9 it is evident that the MD simulations which account for the excluded volume effects are closest to the experimental data.

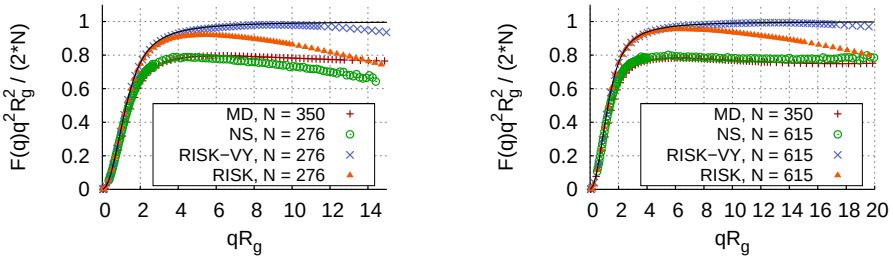

Figure 6.9: The plots show that the RIS-MC model does not correctly reflect the chain structure of PIB in the melt. The form factor of the MD-simulated PIB fits better.

7 | Retrospective

Neutron and x-ray scattering data of polymer coils in the melt or theta solution are commonly compared to the form factor of chains generated by the rotational isomeric state model (RIS). The RIS method which is discussed in 4.3 generates chains, which neglect excluded volume effects but are true to chemical detail. The foundation of the RIS theory lies within Flory's' ideality hypothesis which states that all excluded volume interaction is screened by the melt. In 1983 Hayashi et al. published a comparison between neutron scattering data and RIS theory for the form factor of polyisobutylene (PIB) [17]. The good agreement of RIS chains with the experimental data reinforced Flory's ideality hypothesis. However, the RIS analysis in [17] is not as convincing as it might seem. As pointed out by DeBolt and Suter, it employed a wrong assignment of the backbone angles. In their Erratum [38], they propose a revised model, but just state that the new version gives indistinguishable results from the wrong one. However, no plot is given to support this point. Later, Vacatello and Yoon criticize [39] the refinement made by DeBolt and Suter. They argue that the DeBolt-Suter model is not really acceptable because it requires reallocated torsional states quite far from those of the energy minima originally deduced in Ref. [37]. Instead of the 4-state RIS model used in Refs. [17, 37, 38], Vacatello and Yoon (VY) suggest a 6-state RIS model (which is more consistent with our PIB model; see fig. 4.23) and show that this model also yields good agreement with experiment [39].

On the one hand, we have the good agreement between the Vacatello-Yoon RIS model and the Hayashi SANS (small angle neutron scattering) data reinforcing the ideality hypothesis. On the other hand, the current SANS data coincides with molecular dynamics (MD) simulations, strongly suggesting that residual excluded volume effects influence the coil structure. This calls for a reexamination of the Vacatello-Yoon model and the Hayashi SANS data.

In this chapter we discuss the most recent RIS model for PIB published by Vacatello and Yoon [39], and why it describes the scattering data of PIB so well. We also generate RIS chains with the torsional map gained from the MD simulations.

The RIS model by Vacatello and Yoon

In the following we compare the Vacatello-Yoon model with the RIS model which utilizes the probability distributions directly derived from

the MD simulation, and the MD simulations themselves. The RIS model derived from the probability distributions of the MD simulation will be referred to as the c.w. (current work) RIS model.

For the comparison with the SANS data from Hayashi et al. the authors employed a 72×72 resolution of the probability maps, but only published the 6×6 matrices, stating that the chains modeled with the lesser resolution were indistinguishable to those relying on the higher resolved map. Hence to reproduce the Vacatello-Yoon data we utilized the 6×6 probability distributions. The differences between the Vacatello-Yoon torsional probability and the torsional probability of MD simulations is discussed in section 4.3. An additional difference between the two RIS models is that the back bone angles of the Vacatello-Yoon model are not distributed, but fixed to the values of $\theta^a = 110$ and $\theta^g = 126$, as opposed to the current work.

Firstly, we discuss the chain stiffness quantified by the persistence length l_p, as this is a defining characteristic of the coil structure. Given the nature of the RIS chains, their bond-bond orientational correlation function is expected to decay exponentially. We begin the analysis of the models by studying the bond-bond orientational correlation function. This function measures how information decays along the backbone. As in section 3.2 the orientational correlation is measured from the quaternary carbon atoms.

$$P_1(s) = \langle \cos(\pi - \theta) \rangle \, \mathrm{e}^{-s/s_\mathrm{p}} \tag{7.1}$$

which describes the bond-bond orientational correlation function, with s_p being the number of segments per persistence length and $\langle \cos(\pi - \theta) \rangle$ the average over the bond angle distribution. The persistence length l_p is calculated by

$$l_\mathrm{p} = \langle a_\mathrm{b} \rangle \int_0^\infty P_1(s) = \langle a_\mathrm{b} \rangle \langle \cos(\pi - \theta) \rangle s_\mathrm{p} \tag{7.2}$$

with $\langle a_\mathrm{b} \rangle$ the mean length of the monomer. Fig. 7.1 shows the fits of eq. (7.1) to the data of the two RIS models and the molecular dynamics simulation (MD). As is expected, the RIS bond-bond correlation functions decays purely exponential. The MD data, on the other hand, shows a power law deviation indicating the long range interactions facilitated by the incompressibility of the melt. The values of the fit parameters l_p and $\langle \cos(\pi - \theta) \rangle$ together with the average monomer length $\langle a_\mathrm{b} \rangle$ and the calculated persistence length are listed below:

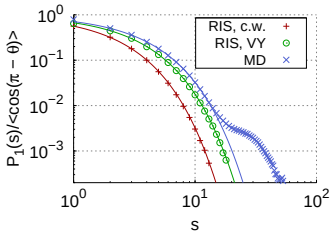

Figure 7.1: The figure shows the bond-bond correlation function of the RIS chains of the current work (c.w.), the reproduced work by Vacatello and Yoon (VY) and the chains simulated with MD methods.

	$\langle a_\mathrm{b} \rangle$ [Å]	$\langle \cos(\pi - \theta) \rangle$	s_p	l_p [Å]
RIS, c.w.	2.77	0.8549	1.74317	4.128
RIS, VY	2.74	0.7819	2.48356	5.321
MD	2.78	0.5835	2.918	4.733

The difference between the MD simulation, which respects the excluded volume, and the c.w. RIS chains, which do not, is noteworthy. If the assumption that the coil structure depends solely on the torsional and angular probability distributions were correct, the properties

of these two chains should be identical. This alone is a indicator that the residual excluded volume affects the coil characteristics.

Neither the RIS model correctly reflects the persistance length. While the c.w. RIS model is too flexible, the Vacatello-Yoon model is too stiff. Flory's characteristic ratio C_∞ can be extracted from the intra chain distance function $R^2(s)/s$ which approaches the squared statistical segment length a_0^2 for $s \gg 1$. The relationship between C_∞ and a_0^2 is

$$C_\infty = \frac{a_0^2}{2\langle l^2 \rangle} \tag{7.3}$$

where $\langle l^2 \rangle$ is the mean square bond length and the factor 2 is the number of backbone bonds per monomer. Fig. 7.2 shows the intra chain distance function of the different models, and the values of C_∞ extracted from this plot are listed below:

	RIS, c.w.	RIS, VY	MD
C_∞	5.21	6.57	6.53

Vacatello and Yoon state that their PIB model delivers a value of $C_\infty = 6.7 \pm 0.2$ which is well within our findings. Even though the MD simulation and the Vacatello-Yoon RIS calculation differ in persistence length, the intrachain distribution function is astonishingly similar. This demonstrates that the coils structure cannot be quantified by one feature alone.

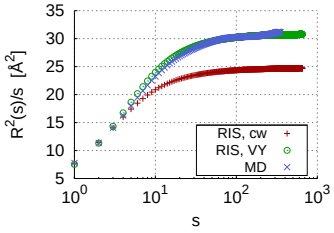

Figure 7.2: The figure shows the intrachain distance function for the three systems.

SANS Data

The good agreement between experimental data and RIS theory is what ratifies Flory's ideality hypothesis. In the following we reexamine the conclusion made over three decades ago. First we compare the SANS measurements done in the scope of this work to the two RIS models and the MD simulations in fig. 7.3. The scattering data is collected from fully deuterated PIB chains, hence the form factor of the simulated data is also calculated from all of the explicit hydrogen atoms. From fig. 7.3 it is clear that neither RIS models fit the experimental scattering picture. The height of the Kratky plateau is below 1 for the

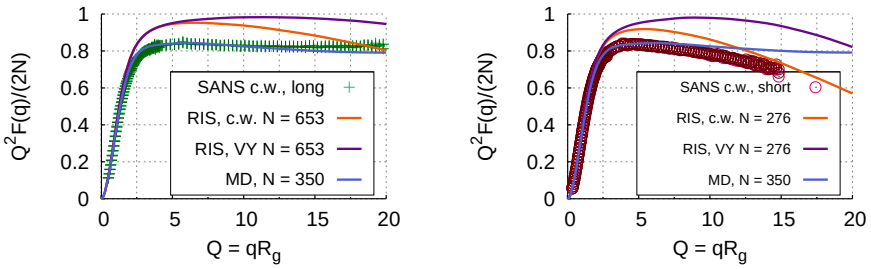

Figure 7.3: The form factor of the two RIS models, the MD data and the SANS data collected in the scope of this work are compared in a normalized Kratky plot. The chain length of the RIS models is chosen to be equivalent with the chain lengths of the real samples (cf. table 5.11).

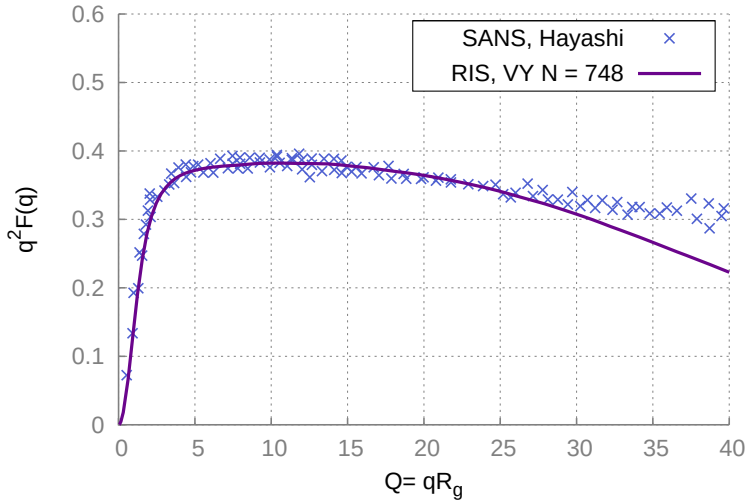

Figure 7.4: The SANS measurements by Hayashi et al. are well described by the RIS model proposed by Vacatello and Yoon of chains of comparable length. The length of the RIS chains is chosen to be comparable with the polymers studied by by Hayashi et al. and the potentials of the RIS model correspond to $T = 400\,\mathrm{K}$.

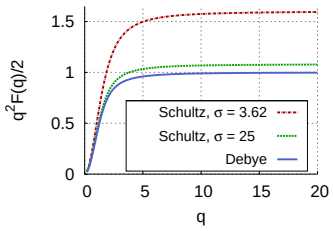

Figure 7.5: The Debye and Debye-Schultz function for different degrees of polydispersity. The weighing factor of $\sigma = 3.62$ is approximately that of Hayashi's samples, and $\sigma = 25$ that of Dadmun's data.

experimental data as well as for the MD data. The depression of the Kratky plateau is an effect of the non-ideality, as is discussed in section 5.1.1. Though our data is seemingly conclusive, the question remains why the SANS data of Hayashi [17] is in such good agreement with the RIS calculations of Vacatello and Yoon. In fig. 7.4 the data of Ref. [17, fig. (8)] is reproduced together with the form factor of RIS chains generated with the method proposed by Vacatello and Yoon [39]. The RIS model coinsides very well with the SANS data. This seemingly contradicts the insight gained from fig. 7.3. In [17] the autors specify that the PIB samples have a polydispersity of $N_\mathrm{w}/N_\mathrm{n} = 1.2763$, where Nn is the number average and N_w is the weight average degree of polymerization. The influence of the polydispersity on the form factor can be estimated. For this purpose we assume the chain lengths to be Schulz distributed. This assumption has also been made in Ref. [17] and can be rationalized by the reaction mechanisme used in the synthesis of PIB. The Debye function that describes the form factor of ideal chain can be weight-averaged over the, presumably Schulz-distributed-polydispersity [75, p. 72-75]. The weighing factor of the Debye-Schulz equation

$$D_\sigma(Q) = N_\mathrm{n} \frac{2}{\left[1/(1+2/\sigma)\right]^2 Q^4} \times \left[\left(1 + \frac{Q^2}{\sigma(1+2/\sigma)}\right)^{-\sigma} - 1 + \frac{Q^2}{1+2/\sigma}\right] \tag{7.4}$$

is related to the polydispersity by

$$\sigma = \frac{1}{(N_\mathrm{w}/N_\mathrm{n}) - 1}\,. \tag{7.5}$$

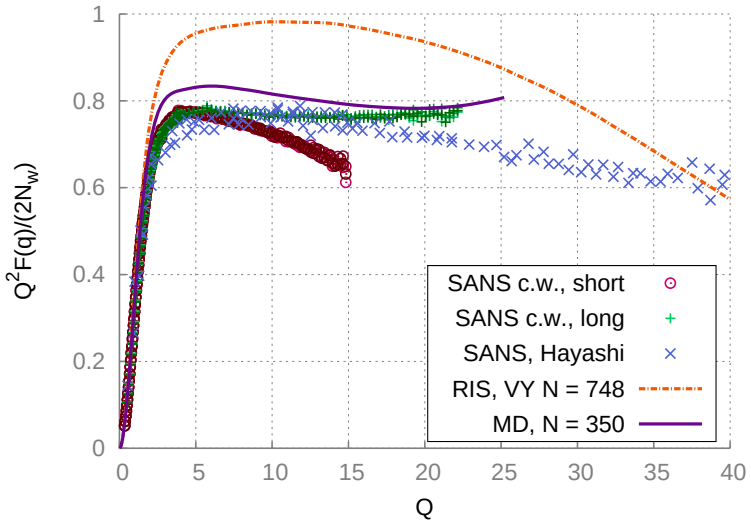

Figure 7.6: The SANS data from Hayashi and that of Dadmun are normalized by there polydispersity. Thoug this is just a rough estimate, the data fit better together.

Fig. 7.5 shows the Debye-Schultz function for varying degrees of polydispersity. The figure shows, that the level of the Kratky plateau converges towards $1 + 2\sigma^{-1}$.

In a hand-waving argument we normalize the SANS data of Hayashi and Dadmun by their respective polydispersities and plot them together. Though the corrected height of the Hayashi Kratky plateau cannot be taken all to seriously, the plot shows that both sets of data are considerably below the RIS data and much better approximated by the MD simulations. This further reinforces that the incomplete screening of the exluded volume influences the coil structure. RIS calculations which do not account for the excluded volume effects are not suitable to correctly predict the coil structure. Hence, even for static properties MD simulations are indispensable.

8 | Conclusion

In this thesis the effects of residual excluded volume interactions among real polymers in a dense melt were studied and successfully shown in atomistically realistic simulations and small angle neutron scattering (SANS) experiments. We successfully employed fine graining to reach equilibrium in very long chains. Computationally the greatest challenge was to generate fully equilibrated systems of atomistically realistic polymers. We tested a number of different methods of which fine graining proved to be the most effective. By developing a coarse-grained system with similar characteristics to PIB we utelized fine-grained to map the chemical detail onto the coarse-grained beads. With this method it was possible to simulate chains of length $N = 350$ — over four times longer then PIB chains that have been simulated to this date. From these simulations we were able to show the non-ideality effects that manifest them selves in the bond-bond orientation correlation function. It is the first time these deviations from ideality have been shown for a realistic polymer model and compared with real polymers.

With the help of the molecular dynamics simulations we could successfully analyze the SANS data collected by our collaborators, M. Dadmun et al. From the SANS data we could also derive the corrections to ideality, albeit only quantitatively, since the existing theory only takes string-like chains into account. These findings give confidentiality to the residual excluded volume theory. The SANS experiments from 1983 that once gave weight to Flory's ideality hypothesis were revisited and the rotational isomeric state simulations that accompanied them reproduced. By estimating the influence of polydispersity on the scattering picture it is possible to show that the 1983 data is in fact closer to the prognosticated non-ideal chains then it is to the ideal chains.

This thesis was successfully in bridging the gap between theory and experiment, but there remains work to be done. Firstly the theory of residual excluded volume effects should be widened to included chains with finite monomer cross-section. Experimentally it is possible to synthesize longer chains then what was studied in this thesis. The longer the chains are, the easier it is to distinguish the effect of non-ideality, so more SANS measurements with longer chains should be performed. Powerful SANS machines are now available at several large scale neutron facilities and even more are anticipated to be installed at the European Spallation Source, such that comparison between theory and experiment is expected to make good progress in the near future.

9 | Acknowledgement

I would like to express my thanks to all who helped bring this work to fruition.

First of all, my sincere thanks go to my supervisor Dr. Joachim Wittmer who walked the long journey with me. He gave me continuous advice, encouragement and support during the study period.

Special thanks go to Prof. Dr. Jörg Baschnagel for his intellectual support and unfailing willingness to discuss all aspects of this thesis. His unfaltering believe in the beauty of polymer physics and his capability to explicate even the most abstract issues were essential for the progress of this thesis.

I am deeply grateful to Dr. Hendrik Meyer for sharing his profound knowledge of numerical methods in polymer science, especially molecular dynamics simulations. He always afforded plenty of time to discuss my analysis and was especially supportive in the tedious process of finding a suitable coarse-grained model for polyisobuthylene.

Dr. Olivier Benzerara's abiding computational and technical support helped me to overcome quite some difficulties and his willingness to share my enthusiasm kept me motivated; I am very grateful to him.

I would like to thank Dr. Christiane Alba-Simionesco, Prof. Dr. Jean-Paul Ryckaert and Dr. Michel Rawiso for accepting to serve on the jury of this thesis.

The thesis has been carried out at the Institut Charles Sadron, Centre National de la Recherche Scientifique. I want to thank the Agence Nationale de la Recherche project "FqSimPIB" for financial support. I highly appreciate the support and favorable working conditions at the ICS.

Most of all I would like to thank my family for their ongoing love, support, encouragement and understanding. They gave me both roots and wings.

Bibliography

[1] Doi M. and Edwards S.F. *The Theory of Polymer Dynamics*. Oxford University Press Inc., New York, 1986.

[2] Colby P. J. and Rubinstein M. *Polymer Physics*. Oxford University Press Inc., New York, 2003.

[3] Flory P. J. *Statistical Mechanics of Chain Molecules*. Wiley, New York, 1969.

[4] Semenov A. N. and Johner A. Theoretical notes on dense polymers in two dimensions. *European Physical Journal E*, 12:469–480, 2003.

[5] Beckrich P., Johner A., Semenov A. N., Obukhov S. P., Benoît H. C., and Wittmer J. P. Intramolecular Form Factor in Dense Polymer Systems: Systematic Deviations from the Debye formula. *Macromolecules*, 40:3805, 2007.

[6] Wittmer J. P., Meyer H., Baschnagel J., Johner A., Obukhov S., Mattioni L., Müller M., and Semenov A. N. Long Range Bond-Bond Correlations in Dense Polymer Solutions. *Physical Review Letters*, 93:147801, 2004.

[7] Wittmer J. P., Beckrich P., Johner A., Semenov A. N., Obukhov S. P., Meyer H., and Baschnagel J. Why polymer chains in a melt are not random walks. *Europhysics Letters*, 77(5):56003, 2007.

[8] Wittmer J.P., Beckrich P., Meyer H., Cavallo A., Johner A., and Baschnagel J. Intramolecular long-range correlations in polymer melts: The segmental size distribution and its moments. *Physical Review E*, 76:011803, 2007.

[9] Meyer H., Wittmer J. P., Kreer T., Beckrich P., Johner A., Farago J., and Baschnagel J. Static Rouse modes and related quantities: Corrections to chain ideality in polymer melts. *European Physical Journal E*, 26, 2008.

[10] Frick B., Richter D., and Trevino S. Inelastic fast relaxation in a weakly fragile Polymer Glass near T(g). *Physica A*, 201:88, 1993.

[11] Angell C. A. Formation of Glasses frin Liquids ans Biopolymers. *Science*, 267:1924, 1995.

[12] Boyd R. H. and Pant P. V. K. Molecular Packing and Diffusion in Polyisobutylene. *Macromolecules*, 24:6325, 1991.

[13] Puskas J. E. and Chen Y. H. Biomedical Application of Commercial Polymers and Novel Polyisobutylene-Based Thermoplastic Elastomers for Soft Tissue Replacement. *Biomacromolecules*, 5:1141, 2004.

[14] Londono J. D., Habenschuss A., Curro J. G., and Rajasekaran J. J. Short-range order in some polymer melts from x-ray diffraction. *Journal of Polymer Science, Part B: Polymer Physics*, 34:3055, 1996.

[15] Weinhold J. D., Curro J. G., Habenschuss A., and Londono J. D. Self-Consistent Integral Equation Theory of Polyolefins and Comparison to X-ray Scattering Experiments. *Macromolecules*, 32:7276, 1999.

[16] Pütz M., Curro J. G., and Grest G. S. Self-consistent integral equation theory for polyolefins: Comparison to molecular dynamics simulations and x-ray scattering. *Journal of Chemical Physics*, 114:2847, 2001.

[17] Hayashi H., Flory P. J., and Wignall G. D. Configuration of Polyisobutylene Chain according to Neutron and X-ray Scattering. *Macromolecules*, 16:1328, 1983.

[18] Frick B., Dosseh G., Cailliaux A., and Alba-Simionesco C. Pressure dependence of the segmental relaxation of polybutadiene and polyisobutylene and influence of molecular weight. *Journal of Chemical Physics*, 292:311, 2003.

[19] Richter D., Monkenbusch M., Arbe A., and Colmenero J. Neutron scattering and the glass transition in polymers - present status and future opportunities. *Journal of Non-Crystalline Solids*, 287:286, 2001.

[20] Arrighi V., Triolo A., and Qian H. Temperature dependence of the segmental dynamics in polyisobutylene melts. *Journal of Non-Crystalline Solids*, 307:654, 2002.

[21] Farago B., Arbe A., Colmenero J., Faust R., Buchenau U., and Richter D. Intermediate length scale dynamics of Polyisobutylene. *Physical Review E*, 65:051803, 2002.

[22] Richter D., Monkenbusch M., Allgeier J., Arbe A., Colmenero J., Farago B., Bae Y. C., and Faust R. From Rouse dynamics to local relaxation: A neutron spin echo study on polyisobutylene melts. *Journal of Chemical Physics*, 111:6107, 1999.

[23] Arbe A., Monkenbusch M., Stellbrink J., Richter D., Farago B., Almdal K., and Faust R. Origin of Internal Viscosity Effects in Flexible Polymers: A Comparative Neutron Spin-Echo and Light

Scattering Study on Poly(dimethylsiloxane) and Polyisobutylene. *Macromolecules*, 34:1281, 2001.

[24] Tanaka A. and Ishida Y. Relationship Between Dielectric Behavior and Molecular Conformation of Polyisobutylene in the Rubbery State. *Journal of Polymer Science Part B: Polymer Physics*, 12:1283, 1974.

[25] Richter D., Arbe A., Colmenero J., Monkenbusch M., Farago B., and Faust R. Molecular Motions in Polyisobutylene: A Neutron Spin-Echo and Dielectric Investigation. *Macromolecules*, 31:1133, 1998.

[26] Bandis A., Wen W. Y., Jones E. B., Kaskan P., Zhu Y., Jones A. A., Inglefield P. T., and Bendler J. T. An NMR Study of Segmental Motion in Poly(isobutylene) and the Relationship to Translational Diffusion of Sorbed CO_2. *Journal of Polymer Science Part B: Polymer Physics*, 32:1707, 1994.

[27] Delabatie R. D., Laupretre F., and Monnerie L. Carbon-13 NMR Investigation of Local Dynamics in Bulk Polymers at Temperatures Well above the Glass-Transition Temperature. 4. Polyisobutylene. *Macromolecules*, 22:2617, 1989.

[28] Karatasos K., Ryckaert J. P., Ricciardi R., and Laupretre F. Methyl Dynamics and β-Relaxation in Polyisobutylene: Comparison between Experiment and Molecular Dynamics Simulations. *Macromolecules*, 35:1451, 2002.

[29] McGrath K. J., Ngai K. L., and Roland C. M. Temperature dependence of segmental motion in polyisobutylene and poly(vinylethylene). *Macromolecules*, 25:4911, 1992.

[30] Kilburn D., Wawryszczuk J., Dlubek G., Pionteck J., Hassler R., and Alam M. A. Temperature and Pressure Dependence of the Free Volume in Polyisobutylene from Positron Lifetime and Pressure-Volume-Temperature Experiments. *Macromolecular Chemistry and Physics*, 207:721, 2006.

[31] Fetters L. J., Graessley W. W., and Kiss A. D. Viscoelastic properties of polyisobutylene melts. *Macromolecules*, 24(11):3136–3141, 1991.

[32] Ngai K. L., Plazek D. J., and Echeverria I. Viscoelastic Properties of Amorphous Polymers. 6. Local Segmental Contribution to the Recoverable Compliance of Polymers. *Macromolecules*, 29:7937, 1996.

[33] Plazek D. J., Chay I. C., Ngai K. L., and Roland C. M. Viscoelastic properties of polymers. 4. thermorheological complexity of the softening dispersion in polyisobutylene. *Macromolecules*, 28:6432, 1995.

[34] Hoeve C. A. Unperturbed Chain Dimensions of Polymeric Chains. *Journal of chemical physics*, 32:888, 1960.

[35] Madkour T. M., Mohammed O. I., and Ebaid A. H. Molecular modeling of polyisobutylene. application of the modified rotational isomeric states model for polymers comprising four rotational isomeric states. *Journal of Macromolecular Science, Physics*, B39:679, 2000.

[36] Boyd R. H. and Breitling S. M. Conformational Properties of Polyisobutylene. *Macromolecules*, 5:1, 1972.

[37] Suter U. W., Saiz E., and Flory P. J. Conformational characteristics of polyisobutylene. *Macromolecules*, 16(8):1317–1328, 1983.

[38] Suter U. W., Saiz E., and Flory P. J. Conformational characteristics of polyisobutylene: an error with consequences. *Macromolecules*, 20(6):1424–1425, 1987.

[39] Vacatello M. and Yoon D. Y. Conformational statistics of polyisobutene by a Monte Carlo study. *Macromolecules*, 25(9):2502–2508, 1992.

[40] Tsolou G., Vlasis G., Mavrantzas G., Makrodimitri Z. A., Economou I. G., and Gani R. Atomistic Simulation of the Sorption of Small Gas Molecules in Polyisobutylene. *Macromolecules*, 41:6228– 6238, 2008.

[41] Qin J. and Morse D. C. Renormalized one-loop theory of correlations in polymer blends. *Journal of chemical physics*, 130:224902, 2009.

[42] Semenov A. N. and Rubinstein M. Dynamics of strongly entangled polymer systems: activated reptation. *European Physical Journal B*, 1:87–94, 1998.

[43] Jones R. L., Kumar S. K., and Ho D.L. Chain conformation in ultrathin polymer films. *Nature*, 400:146–149, 1999.

[44] Shin K., Obukhov S., Chen J. T., Huh J., Hwang Y., Mok S., Dobriyal P., Thiyagarajan P., and Russell T. P. Enhanced mobility of confined polymers. *Nature Materials*, 6:961–965, 2007.

[45] Nath S. K. and Khare R. New forcefield parameters for branched hydrocarbons. *Journal of Chemical Physics*, 115:10837, 2001.

[46] Plimpton S. Fast parallel algorithms for short-range molecular-dynamics. *Journal of Computational Physics*, 117:1–19, 1995.

[47] Lorentz H. A. Ueber die Anwendung des Satzes vom Virial in der kinetischen Theorie der Gase. *Annalen der Physik*, 248:127–136, 1881.

[48] Berthelot D. Sur le mélange des gaz. *Comptes rendus hebdomadaires des séances de l'Académie des Sciences*, 126:1703–1855, 1898.

[49] Andersen H. C. RATTLE - a velocity version of the SHAKE algorithm for molecular-dynamics calculations. *Journal of Computational Physics*, 52:24, 1983.

[50] Tanaka T., Chatani Y., and Tadokoro H. Crystal structure of polyisobutylene. *Journal of Polymer Science, Part B: Polymer Physics*, 12:515–531, 1974.

[51] Strobl G. R. *The Physics of Polymers, 2nd Edition*. Springer-Verlag, Berlin, Heidelberg, New York, 1997.

[52] Shinoda W., Shiga M., and Mikami M. Rapid estimation of elastic constants by molecular dynamics simulation under constant stress. *Physical Review B*, 69:134103, 2004.

[53] Tuckerman M. E., Alejandre J., Lopez-Rendon R., Jochim A. L., and Martyna G. J. A Liouville-operator derived measure-preserving integrator for molecular dynamics simulations in the isothermal-isobaric ensemble. *Journal of Physics A*, 39(19):5629, 2006.

[54] Eichinger B. E. and Flory P. J. Determination of the Equation of State of Polyisobutylene. *Macromolecules*, 1(3):285–286, 1968.

[55] Ghanbari A., Bohm M., and Muller-Plathe F. A Simple Reverse Mapping Procedure for Coarse-Grained Polymer Models with Rigid Side Groups. *Macromolecules*, 44(13):5520–5526, 2011.

[56] Carbone P., Karimi-Varzaneh H. A., and Mueller-Plathe F. Fine-graining without coarse-graining: an easy and fast way to equilibrate dense polymer melts. *Faraday Discussions*, 144:25–42, 2010.

[57] Weeks J. D., Chandler D., and Andersen C. H. Role of repulsive forces in determining the equilibrium structure of simple liquids. *Journal of Chemical Physics*, 12:5237–5247, 1971.

[58] Lide D. E. *CRC Handbook of Chemistry and Physics*. CRC Press, Boca Raton, FL, Internet Version 2005.

[59] Flory P. J. Foundations of Rotational Isomeric State Theory and General Methods for Generating Configurational Averages. *Macromolecules*, 7(3):381–392, 1974.

[60] Kirkpatrick S. and Stoll E. P. A very fast Shift-Register Sequence random number generator. *Journal of Computational Physics*, 40:517–526, 1981.

[61] Press W. H., Teukolsky S. A., and Vetterling W. T. an Flannery B. P. *Numerical Recipes in Fortran 77*. Cambridge University Press, Cambridge, 1992.

[62] Baschnagel J., Binder K., Paul W., Laso M., Suter U. W., Batoulis I., Jilge W., and Burger T. On the construction of coarsegrained models for linear flexible polymer chains: Distribution functions for groups of consecutive monomers. *Journal of Chemical Physics*, 95:6014, 1991.

[63] Higgins J. S. and Benoît H. C. *Polymers and Neutron Scattering*. Oxford University Press Inc., New York, reprinted (with corrections), 1997 edition, 1994.

[64] Mortensen K. Structural studies of polymer systems using small-angle neutron scattering. *Advanced functional molecules and polymers*, 2:223–269, 2011.

[65] Rawiso M., Duplessix R., and Picot C. Scattering function of polystyrene. *Macromolecules*, 20(3):630–648, 1987.

[66] Bates F. S. and Wignall G. D. Non-ideal mixing in binary blends of perdeuterated and protonated polystyrenes. *Macromolecules*, 19(3):932–934, 1986.

[67] Beaucage G., Sukumaran S., Clarson S. J., Kent M. S., and Schaefer D. W. Symmetric, Isotopic Blends of Poly(dimethylsiloxane). *Macromolecules*, 29(26):8349–8356, 1996.

[68] Wittmer J. P., Cavallo A., Xu H., Zabel J. E., Polinska P., Schulmann N., Meyer H., Farago J., Johner A., Obukhov S. P., and Baschnagel J. Scale-Free Static and Dynamical Correlations in Melts of Monodisperse and Flory-Distributed Homopolymers A Review of Recent Bond-Fluctuation Model Studies. *Journal of Statistical Physics*, 145(4):1017–1126, 2011.

[69] Grosberg A. Y. and Khokhlov A. R. *Giant Molecules - Here, There and Everywhere*. Worl Scientific Publishing Co. Pte. Ltd., 5 Toh Tuck Link, Singapore 596224, 2nd edition, 2011 edition, 1997.

[70] de Gennes P.-G. *Scaling Concepts in Polymer Physics*. Cornell University Press, Sage House, 512 East State Street, Ithaca, New York, fifth printing, 1996 edition, 1979.

[71] Müller M., Binder K., and Schäfer L. Intra- and Interchain Correlations in Semidilute Polymer Solutions: Monte Carlo Simulations and Renormalization Group Results. *Macromolecules*, 33(12):4568–4580, 2000.

[72] Semenov A. N. and Obukhov S. P. Fluctuation-induced long-range interactions in polymer systems. *European Physical Journal E*, 17:S1747–S1775, 2005.

[73] Wittmer J. P., Meyer H., Schulmann N., Zabel J. E., and Johner A. The generalized Porod law and compact polymer structures. *European Physical Journal E*, 2010. in preparation.

[74] Semenov A. N. and Nyrkova I. A. 1.02 - Statistical Description of Chain Molecules. In K. Editors-in Chief: Matyjaszewski and M. Müller, editors, *Polymer Science: A Comprehensive Reference*, pages 3 – 29. Elsevier, Amsterdam, 2012.

[75] Schäfer L. *Excluded Volume Effects in Polymer Solutions*. Springer-Verlag, Berlin-Heidelberg, 1999.